Coincidence Measurements of Single-Pion Electroproduction near the $\Delta(1236)$ Resonance*

C. MISTRETTA,† J. A. APPEL,‡ R. J. BUDNITZ,§ L. CARROLL,‖ J. CHEN, J. R. DUNNING, JR., M. GOITEIN,** K. HANSON, D. C. IMRIE,†† AND RICHARD WILSON
Physics Department, Harvard University, Cambridge, Massachusetts 02138

Differential cross sections for the reactions $e^-+p \rightarrow e^-+p+\pi^0$ and $e^-+p \rightarrow e^-+n+\pi^+$ have been measured near the $\Delta(1236)$ resonance at four-momentum transfers of 0.05, 0.13, 0.25, and 0.4 $(\mathrm{GeV}/c)^2$. A few measurements of the π^+ angular distribution have been obtained at a four-momentum transfer of 0.6 $(\mathrm{GeV}/c)^2$. Cross sections for the π^0 reaction are compared with dispersion-theory predictions at several pion-nucleon c.m. energies for each four-momentum transfer. A phenomenological analysis of the π^0 results leads to the determination of the magnetic dipole and electric quadrupole partial-wave amplitudes and the $\gamma N\Delta$ transition form factor. Evidence is found for the existence of a significant scaler-transverse interference term in the cross section, which is tentatively associated with the resonant scaler quadrupole interaction. Cross sections for π^+ electroproduction are compared with dispersion theories using the pion form factor as a free parameter. The results suggest a form factor similar to that of the proton. A fit to the form-factor results, using the ρ-dominance model, requires $m_\rho = 560 \pm 80$ MeV. The rms pion charge radius is estimated to be $\langle r^2 \rangle^{\frac{1}{2}} = 0.86 \pm 0.14$ F.

I. INTRODUCTION

THE first measurements of high-energy inelastic electron scattering from hydrogen were performed by Panofsky and collaborators between 1956 and 1958.[1] Later experiments, in which only the scattered electron has been detected, have explored the region of pion-nucleon c.m. energy from the single pion threshold to above the $\Delta(1236)$ resonance in considerable detail, at four-momentum transfers below 0.8 $(\mathrm{GeV}/c)^2$.[2-4] During the same period, other laboratories have investigated the excitation of the $\Delta(1236)$ and higher pion-nucleon resonances at four-momentum transfers up to 3.6 $(\mathrm{GeV}/c)^2$.[5-7] In addition, a limited number of measurements of the single pion electroproduction reaction $e^-+p \rightarrow e^-+p+\pi^0$, in which the final-state proton has been detected in coincidence with the scattered electron, have been obtained by several groups.[6,8,9]

In 1959, Frazer[10] pointed out that a measurement of the pion form factor could be obtained by extrapolating angular distribution measurements of the reaction $e^-+p \rightarrow e^-+n+\pi^+$ to the one-pion-exchange (OPE) pole. So far, the experimental accuracy necessary for this extrapolation has not been achieved. However, Akerlof *et al.*[11] have exploited the dominance of a longitudinal contribution to the cross section in the above reaction due to OPE to obtain a measurement of the pion form factor. Akerlof *et al.* made measurements at several electron scattering angles in an effort to isolate the longitudinal contribution to the cross section, but, because of the difficulties associated with large-angle electron-scattering coincidence measurements, the separation was not possible and it was necessary to rely on the dispersion theory of Zagury[12] in order to estimate the pion form factor. The variation of the cross section with electron-scattering angle supported the hypothesis of a large longitudinal contribution to the cross section, but the values obtained for the pion form factor depended, almost entirely, upon the small-angle measurements.

Until the precision required for an extrapolation to the pole can be achieved, measurements of the pion form factor based on electroproduction experiments must rely heavily upon theoretical estimates of backgrounds to the OPE contribution. Objections to the whole electroproduction approach can only be answered by a detailed comparison of available theories with

* Work supported by the U. S. Atomic Energy Commission.
† Presently at the University of Wisconsin, Madison, Wis.
‡ Partially supported by a Danforth Foundation Graduate Fellowship.
§ Presently at Lawrence Radiation Laboratory, University of California, Berkeley, Calif.
‖ Presently at Liverpool University, Liverpool, England.
** Partially supported by a Frank Knox Memorial Fellowship and by an I.B.M. Fellowship.
†† Permanent address: University College London, London, England.

[1] W. K. H. Panofsky, W. M. Woodward, and G. B. Yodh, Phys. Rev. **102**, 1392 (1956); W. K. H. Panofsky and E. Allton, *ibid.* **110**, 1155 (1958).
[2] L. N. Hand, Phys. Rev. **129**, 1834 (1963); and Ph. D. thesis, Stanford University, Stanford, California, 1961 (unpublished).
[3] H. L. Lynch, J. V. Allaby, and D. M. Ritson, Phys. Rev. **164**, 1635 (1967).
[4] C. Betourne, C. Feautrier, J. Perez-y-Jorba, and D. Treille, Nucl. Phys. **B5**, 355 (1968).
[5] A. A. Cone, K. W. Chen, J. R. Dunning, Jr., G. Hartwig, Norman F. Ramsey, J. K. Walker, and Richard Wilson, Phys. Rev. **156**, 1490 (1967).
[6] F. W. Brasse, J. Engler, E. Ganssauge, and M. Schweizer, Nuovo Cimento **55A**, 679 (1968).
[7] W. Bartel, B. Dudelzak, H. Krehbiel, J. McElroy, U. Meyer-Berkhout, W. Schmidt, V. Walther, and G. Weber, Phys. Letters **28B**, 148 (1968).
[8] K. Baba, N. Kajiura, S. Kaneko, K. Hake, R. Kikuchi, Y. Kobayashi, and T. Yamakawa, in *Proceedings of the 1967 International Symposium on Electron and Photon Interactions at High Energies* (Stanford Linear Accelerator Center, Stanford, Calif., 1967), p. 102; and I. N. S. (Japan) Report, 1968 (unpublished).
[9] C. W. Akerlof, W. W. Ash, K. Berkelman, and M. Tigner, Phys. Rev. Letters **14**, 1036 (1965).
[10] W. R. Frazer, Phys. Rev. **115**, 1763 (1959).
[11] C. W. Akerlof, W. W. Ash, K. Berkelman, A. C. Lichtenstein, A. Ramanauskas, and R. H. Siemann, Phys. Rev. **163**, 1482 (1967).
[12] N. Zagury, Phys. Rev. **145**, 1112 (1966).

TABLE I. Summary of kinematic regions covered by the coincidence measurements of inelastic electron-proton scattering. The asterisk indicates that angular distribution measurements have been made for the kinematic region listed in columns 1–6.

q^2 (GeV/c)^2	K (GeV)	W (GeV)	E (GeV)	θ_e (°)	ϵ	$e^-+p\rightarrow e^-+p+\pi_0$	$e^-+p\rightarrow e^-+n+\pi^+$
0.0483	0.260	1.170	2.001	6.77	0.981		*
0.0475	0.294	1.197			0.978	*	*
0.0463	0.328	1.223			0.974	*	*
0.132	0.276	1.183	3.264	6.76	0.987	*	*
0.130	0.332	1.226			0.984	*	*
0.127	0.391	1.270			0.982	*	*
0.255	0.214	1.132	4.515	6.67	0.990	*	
0.252	0.255	1.166			0.989	*	
0.250	0.298	1.200			0.988	*	*
0.247	0.334	1.228			0.987	*	
0.245	0.376	1.259			0.986	*	*
0.243	0.409	1.284			0.985	*	
0.240	0.461	1.321			0.984	*	
0.404	0.343	1.232	4.507	8.64	0.980	*	*
0.398	0.403	1.278			0.978	*	*
0.595	0.416	1.289	5.019	9.55	0.974		*

measurements of both π^0 and the π^+ reactions over a wide kinematic range.

In the present paper, coincidence measurements of the angular distributions for the reactions $e^-+p\rightarrow e^-+p+\pi^0$ and $e^-+p\rightarrow e^-+n+\pi^+$ are presented for pion-nucleon c.m. energies in the region of the $\Delta(1236)$ resonance at four-momentum transfers near 0.05, 0.13, 0.25 and 0.4 (GeV/c)^2. A limited amount of π^+ data have been obtained at a four-momentum transfer of 0.6 (GeV/c)^2. Summaries of the results have been published elsewhere.[13,14]

In addition to permitting a detailed test of the theories, the π^0 data have provided a good deal of reasonably model-independent dynamical information.[15] The assumption of the dominance of S and P pion-nucleon partial waves at c.m. energies below 1350 MeV has led to a determination of the resonant magnetic dipole amplitude and the electric quadrupole amplitude. The phenomenological description of the Δ as a particle excited by magnetic dipole radiation leads to the definition of a $\gamma N\Delta$ form factor, which has been evaluated for four-momentum transfers up to 0.4 (GeV/c)^2. The π^0 data also provide some evidence for the existence of the resonant scalar quadrupole amplitude at four-momentum transfers of 0.13 and 0.25 (GeV/c)^2.

The π^+ data have been analyzed in terms of the pion form factor in a manner similar to that employed by Akerlof *et al.* Although the form-factor values have been derived from more extensive data, they are subject to the same systematic errors as those encountered by the Cornell group. However, the results, which are in satisfactory agreement with the earlier data, have been interpreted with both of the presently available theories and have been assigned larger theoretical error to allow for differences in the dispersion models.

A summary of the kinematic range of the coincidence data is given in Table I. The π^0 data cover polar angles (measured relative to the three-momentum transfer to the pion-nucleon system) between 120° and 170° c.m., approximately, and azimuthal angles between 30° and 170°. The π^+ data cover a slightly more limited range of azimuthal angle, for polar angles between zero and 40° c.m.

Electroproduction theory and related topics are discussed in Sec. II. The apparatus is described in Sec. III, and experimental procedures associated with data collection and analysis are described in Secs. IV and V. Elastic cross-section values and noncoincidence inelastic scattering cross sections, which were measured periodically during the course of the experiment, are summarized in Sec. VI. The results for the π^0 and π^+ coincidence measurements are discussed in Secs. VII and VIII, respectively. Section IX considers improvements in experimental techniques which might be incorporated in future experiments and suggests directions for extending the work presented here. The differential cross sections measured in this experiment are too numerous to present here and will be made available elsewhere.[16]

II. ELECTROPRODUCTION THEORY AND RELATED TOPICS

A. Kinematics

The complete definition of a single-pion coincidence event requires the specification of five quantities (see Fig. 1). From the experimental standpoint, the most convenient are

[13] C. Mistretta, D. Imrie, J. A. Appel, R. Budnitz, L. Carroll, J. Chen, J. Dunning, Jr., M. Goitein, K. Hanson, A. Litke, and R. Wilson, Phys. Rev. Letters **20**, 1070 (1968).

[14] C. Mistretta, D. Imrie, J. A. Appel, R. Budnitz, L. Carroll, M. Goitein, K. Hanson, and Richard Wilson, Phys. Rev. Letters **20**, 1523 (1968).

[15] D. Imrie, C. Mistretta, and Richard Wilson, Phys. Rev. Letters **20**, 1074 (1968).

[16] For this supplementary material, order NAPS Document 00500 from ASIS National Auxiliary Publications Service, % CCM Information Sciences, Inc., 22 West 34th Street, New York, New York 10001; remitting $1 for microfiche or $3 for photocopies.

(1) the incident beam energy E;
(2) the scattered electron energy E';
(3) the electron scattering angle $\theta_{e'}$;
(4) the polar angle $\theta_{\pi,p}$ which the positive pion or proton makes with $\bar{q}$, the three-momentum transfer to the pion-nucleon system; and
(5) the azimuthal angle ϕ_π between the electron scattering plane and the plane defined by $\bar{q}$ and the pion momentum $\bar{\pi}$.

The theoretical analysis of the reaction is simpler when the first three of these are replaced by

(1) q^2, the square of the four-momentum transfer to the π-N system (positive in the metric employed here);
(2) W, the total energy in the π-N system; and
(3) ϵ, the polarization of the transverse components of the virtual photon.

Electroproduction of pions is most easily understood as photoproduction by virtual photons. In order to emphasize this correspondence, it is useful to introduce the variable K, the energy required by a real photon in the laboratory to produce the same pion-nucleon c.m. energy,

$$K=q_0-q^2/2M,$$

where q_0 $(=E-E')$ is the energy transfer in the laboratory, q^2 $(=4EE'\sin^2\frac{1}{2}\theta_e\equiv|\mathbf{q}|^2-q_0^2\geq 0)$ is the invariant square of the four-momentum transfer, and M is the proton mass.

Expressions for other useful quantities, in the limit of zero electron mass, are listed below,

scattered electron energy,

$$E'=(E-K)/[1+(2E/M)\sin^2\tfrac{1}{2}\theta_e]; \tag{1}$$

pion-nucleon c.m. energy,

$$W=(M^2+2KM)^{1/2}.$$

Starred quantities refer to the pion-nucleon c.m. system, e.g.,

energy transfer in the c.m. system,

$$q_0^*=(Mq_0-q^2)/W,$$

three-momentum transfer in the c.m. system,

$$\mathbf{q}^*=M\mathbf{q}/W.$$

B. Virtual Photon Polarization

The only differences between the photoproduction and electroproduction of pions are that in the latter case the photon is virtual ($q^2\neq 0$) and has scalar and longitudinal components. These give rise to interactions which are not possible with real, purely transverse, photons. Because the interactions involving the scalar and longitudinal components are related by current conservation,[17] the nontransverse contributions to the cross section can be discussed be referring to either.

[17] L. N. Hand and R. Wilson, SLAC Report No. 25, Part 2, 1963 (unpublished).

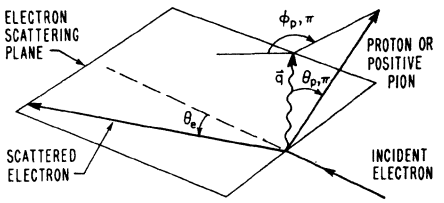

FIG. 1. Diagram illustrating the definition of laboratory frame vectors and angles in single pion electroproduction. The undetected neutral particle is not shown.

We will write down quantities in the scalar notation, but the alternative description often appears in the literature and should be kept in mind.

In experiments where only the final electron is detected, the cross section can be separated into two distinct parts. In the notation of Hand[2]

$$\begin{aligned} d^2\sigma/d\omega_e dE' &= \Gamma_T\sigma_T(q^2,W)+\Gamma_0\sigma_0(q^2,W) \\ &= \Gamma_T[\sigma_T(q^2,W)+\epsilon\sigma_0(q^2,W)], \end{aligned} \tag{2}$$

where

$$\begin{aligned} \Gamma_T &= \frac{\alpha}{4\pi^2}\frac{K}{q^2}\frac{E'}{E}\left(2+\frac{\cot^2\frac{1}{2}\theta_e}{1+q_0^2/q^2}\right), \\ \Gamma_0 &= \frac{\alpha}{4\pi^2}\frac{K}{q^2}\frac{E'}{E}\left(\frac{\cot^2\frac{1}{2}\theta_e}{1+q_0^2/q^2}\right). \end{aligned} \tag{3}$$

Here ω_e is the electron solid angle in the laboratory and $\Gamma_0/\Gamma_T=\epsilon$ is the polarization of the transverse components of the electromagnetic field. At $q^2=0$, the transverse cross section σ_T reduces to the total photoproduction cross section for the same value of K.

For high electron energies and small scattering angles, the transverse components of the electromagnetic field are almost completely polarized in the electron-scattering plane and the same types of experiments which can be done with polarized photon beams can be done with electron scattering. In situations where the scalar interactions do not complicate the interpretation of the data, the fact that the virtual photon polarization is nearly complete, and its energy well determined, can be an asset. In the present series of measurements the polarization was approximately 0.98. The consequences of this are quite evident in the distinct azimuthal asymmetries in the data presented in Secs. VII and VIII.

C. Cross-Section Formula

The triply differential cross section may also be expressed as a product of two factors, one Γ_T, describing the electron-photon vertex[18] and another representing

[18] Two different definitions of the kinematic factor Γ_T exist in the literature. The factor used by Akerlof *et al.* (called Γ_A here) is related to Γ_T by $\Gamma_A=\Gamma_T|\mathbf{q}|/K$, where $|\mathbf{q}|$ is the three-momentum transfer in the laboratory. Since the ratio $(|\mathbf{q}|/K)_{q^2=0}=1$, the two definitions are equivalent in the photoproduction limit. For finite values of q^2 our cross sections σ are related to those of Akerlof *et al.*, σ_A. $\sigma=(|\mathbf{q}|/K)\sigma_A=(|q^*|W/MK)\sigma_A$. The choice of Γ factors is somewhat arbitrary. Our Γ_T agrees with that originally proposed by Hand (Ref. 2) and used by Lynch *et al.* (Ref. 3).

the interaction of the virtual photon with the strongly interacting particles. In an extension of Hand's notation[2] we write

$$d^3\sigma/d\omega_e d\Omega_\pi dE' = \Gamma_T d\sigma/d\Omega_\pi, \quad (4)$$

where Ω_π is the pion solid angle in the π-N c.m. system and

$$\frac{d\sigma}{d\Omega_\pi} = \frac{d\sigma_T}{d\Omega_\pi} + \epsilon \frac{d\sigma_0}{d\Omega_\pi} + \epsilon \sin^2\theta_\pi^* \, T(\theta_\pi^*) \cos 2\phi + [\tfrac{1}{2}\epsilon(\epsilon+1)]^{1/2} S(\theta_\pi^*) \sin\theta_\pi^* \cos\phi_\pi. \quad (5)$$

The first term in Eq. (5) is entirely due to transverse interactions and reduces to the corresponding photoproduction cross section at $q^2=0$. The second term is purely scalar and is absent in photoproduction.

Experiments involving the detection of the scattered electron alone measure the integral of the above two terms over all pion angles, summed over both decay modes of the Δ. The measurements of Lynch *et al.*[3] indicate that the ratio σ_0/σ_T increases with q^2 to a value of 0.37 at $q^2=0.3$ (GeV/c)^2 and then decreases again at higher q^2. A recent measurement by Bétourné *et al.*[4] has indicated a significant scalar cross section at $q^2=0.13$ (GeV/c)^2 near threshold. These measurements are interesting but cannot determine whether the scalar interaction appears in the π^0 or in the π^+ production process.

As noted in Sec. I, the recent work of Berkelman and co-workers at Cornell[11] has shown that there is an appreciable scalar contribution to the π^+ cross section at $\theta_\pi^*=0^0$, which has been interpreted to be due mainly to the presence of the OPE process involving the π^+ form factor.

The third term in the cross section is due to transverse-transverse interference and has been observed with real polarized photons by groups at Stanford[19] and Frascati,[20] and in electroproduction by Akerlof *et al.*[9] at Cornell. This term is quite large and is one of the outstanding features of the data presented here.

The fourth term in the cross section is due to scalar-transverse interference and had not been observed prior to this experiment. It shows up clearly in the π^+ cross sections, where it is expected on the basis of the pion pole diagram. The surprising fact is that it also appears in the π^0 data, which are unaffected by the pion pole term, except through final-state interactions.

D. Dynamics

The form of the cross section discussed above is based on the assumption of one photon exchange and contains no other dynamical assumptions. In order to say more it is necessary to rely on a theoretical model for the interaction of the virtual photon with the strongly interacting particles.

The description of the process as a function of K is, in general, extremely complicated and the backgrounds are not well understood. So far, the only region for which reliable theoretical predictions can be made is that near the well-known $\Delta(1236)$ resonance.

In 1957, Chew, Low, Goldberger, and Nambu[21] (CGLN) described the general features of pion photoproduction in this energy region using the method of dispersion relations. In 1958, the theory was extended to electroproduction by Fubini, Nambu, and Wataghin[22] (FNW). This theory was shown by Hand,[2] in 1963, to be in reasonably good agreement with experimental measurements of pion production up to 0.39 (GeV/c)^2 for the case where only the scattered electron was detected. A comparison of the theory with a set of π^+ differential cross-section measurements was made in 1965[23] following the experiment by Akerlof *et al.*[11] Although these measurements were not a stringent test of the theory, the agreement was surprisingly good.

The early dispersion theories of CGLN and FNW were static models which assumed an infinitely massive nucleon. Their range of application in electroproduction was, therefore, limited to four-momentum transfers below about 0.4 (GeV/c)^2. Two recent calculations have been performed by Zagury[12] and by Adler.[24] The most outstanding improvement offered by these theories is the fully relativistic treatment of nucleon recoil.

In these theories, the pion production amplitude consists of the Born terms, dispersion-integral estimates of the most important partial-wave amplitudes, and an estimate of the final-state interactions involving the rescattering of the pion from the outgoing nucleon. The amplitude contains no free parameters and involves pion-nucleon phase shifts, nucleon form factors, and the pion form factor through the OPE term.

The dominant process in this energy region is the resonant magnetic dipole M_1^+ transition to the 3-3 state (the notation is that of CGLN, where the 1 implies that the pion is in a state with orbital angular momentum $l=1$ and the $+$ implies that the total angular momentum is l *plus* $\frac{1}{2}$). The presence of this amplitude is evident in the angular-distribution measurements for photoproduction, especially for the π^0+p final state.

The π^+ cross section is more complicated and contains appreciable nonresonant contributions from the large S-wave electric dipole amplitude, which dominates π^+ photoproduction near threshold, and the pion pole term. There are many other smaller contributions

[19] D. J. Drickey and R. F. Mosley, Phys. Rev. **136**, B543 (1964).

[20] G. Barbiellini, *et al.*, in *Proceedings of the Sienna International Conference on Elementary Particles and High-Energy Physics, 1963*, edited by G. Bernardini and G. P. Puppi (Società Italiana di Fisica, Bologna, 1963), p. 516.

[21] G. F. Chew, M. L. Goldberger, F. E. Low, and Y. Nambu, Phys. Rev. **106**, 1345 (1957).

[22] S. Fubini, Y. Nambu, and V. Wataghin, Phys. Rev. **111**, 329 (1958).

[23] C. Mistretta, Internal Report, Harvard Cyclotron Laboratory, 1965 (unpublished).

[24] S. L. Adler, Ann. Phys. (N. Y.) **50**, 189 (1968).

to the cross section, some of which have not yet been calculated.

III. APPARATUS

The apparatus, which is shown in Fig. 2, was similar to that used in recent measurements of elastic electron-proton scattering and quasielastic electron-deuteron scattering at Harvard.[25,26]

An external electron beam from the Cambridge electron accelerator was focused upon a liquid-hydrogen target and electrons scattered at the appropriate angle, within a 14% momentum interval centered upon the peak of the $\Delta(1236)$ resonance, were detected in a half-quadrupole magnetic spectrometer. Protons and positive pions were detected in coincidence with scattered electrons by a counter array consisting of three scintillation counters, a 12×12 scintillator hodoscope and a Plexiglas Cerenkov counter, protected from the background flux of low-energy charged particles by a sweeping magnet.

The data associated with each event were processed by an on-line PDP-1 computer and stored on magnetic tape. No attempt was made to separate pions from protons during data taking. Particle identification was accomplished during subsequent analysis using pulse-height information from the first two scintillation counters and the Čerenkov counter of the coincidence array.

A. Electron Beam and Target

The incident electron beam was focused to form a spot, typically 3 mm wide by 1 mm high, at the target position. The size and position of the spot were observed by lowering a carefully surveyed tungstate screen into the electron beam at the target position and viewing the fluorescence with a closed-circuit television system. Unscattered electrons passed through a tuned rf cavity, which monitored the horizontal position of the beam 3 m downstream from the hydrogen target, traversed a 0.4 radiation-length secondary-emission monitor (SEM), and were collected by a well-shielded Faraday cup. The Faraday cup current was transmitted to an integrator circuit which was calibrated to better than 0.1%. The over-all uncertainty in the measurement of the beam flux is estimated to be less than 0.4%. The SEM was used only as a relative monitor to check the long-term stability of the Faraday cup and integrator system.

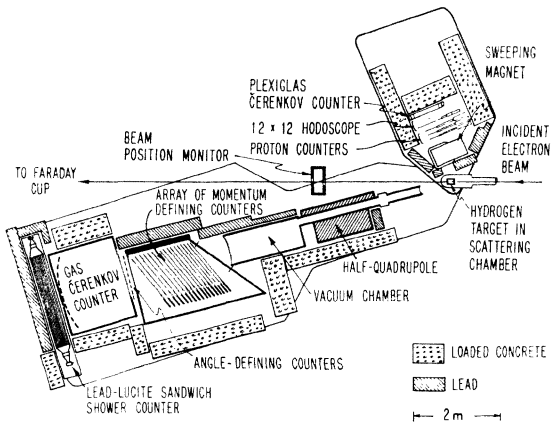

FIG. 2. Plan view of apparatus.

The incident beam passed axially through a cylindrical target cup approximately 5 cm long and 3 cm in diam, constructed of 0.013 cm Mylar with 0.004 cm aluminum end caps. The liquid hydrogen was condensed from tanks of gaseous hydrogen using cold helium gas as a refrigerant. The details of the cryogenic system are described in Ref. 27. Several nominally identical target cups were used throughout the course of the experiment. Their lengths were measured at room temperature and a -0.4% correction was applied to allow for the change in length upon cooling.[25] The number of protons per unit area of the target was calculated using a value of 0.0708 g/cm^3 for the density of liquid hydrogen at 1 atm and is estimated to be in error by less than 0.5%.

B. Electron Spectrometer

The electron spectrometer, which consisted of a half-quadrupole magnet followed by a series of scintillation counters, a Čerenkov counter, and an electron shower counter, has been described in detail by Goitein *et al.*[25] The entire system was mounted on a massive movable platform which could be rotated in the horizontal plane about a pivot situated beneath the center of the target.

The half-quadrupole magnet was a standard CEA 30-cm quadrupole magnet split vertically, with one-half replaced by an iron flux-return piece. A 1.2-m-long lead plug, held centrally in the gap, shielded the scintillation counters in the focal plane from direct line of sight of the target. The electron solid angle was defined in the horizontal plane at the rear of the magnet by a 5-cm-thick lead and tungsten aperture, and in the vertical plane in front of the quadrupole by 1.5-cm-thick, tapered tungsten jaws. Each effective aperture, one corresponding to electrons passing over the central plug, the other to electrons passing below it, subtended a solid angle of approximately 0.4 msr at the target. The error in the electron solid angle is estimated to be 1.2%.

The use of a half-quadrupole magnet allowed small electron scattering angles to be employed, with a consequent increase in the counting rate and in the virtual

[25] M. Goitein, R. Budnitz, J. Appel, L. Carroll, J. Chen, J. R. Dunning, Jr., K. Hanson, D. Imrie, C. Mistretta, J. K. Walker, and Richard Wilson (unpublished).

[26] R. Budnitz, J. Appel, L. Carroll, J. Chen, J. R. Dunning, Jr., M. Goitein, K. Hanson, D. Imrie, C. Mistretta, J. K. Walker, and Richard Wilson, Phys. Rev. 173, 1357 (1968).

[27] M. Goitein, Ph.D. thesis, Harvard University, 1968 (unpublished).

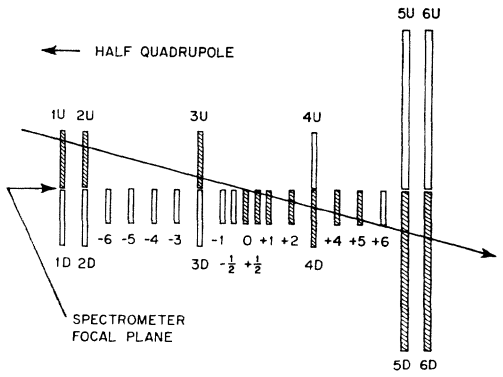

FIG. 3. Side view of momentum defining counters in the electron spectrometrs, illustrating a falling trajectory crossing the center of the focal plane. Triggered counters are shaded.

photon polarization. The minimum attainable electron scattering angle was approximately 6.5°.

Scattered electrons passing through the magnet were focused on to an array of 25 scintillation counters (Fig. 3), which defined the crossing point of trajectories within a momentum band of $\pm 7\%$ about the central momentum determined by the magnet current. The counters defined momentum intervals which were nominally 1% wide, with the exception of four $\frac{1}{2}\%$ bins around the central momentum. The over-all momentum resolution of the spectrometer varied between 1.5 and 3% (full width at half-maximum), depending on the scattered momentum, and led to a resolution of ± 20 MeV in W. The resolution was limited by the length of the target, the vertical extent of the electron beam, and multiple scattering of the scattered electrons.

Directly behind the momentum-defining counters was an array of ten electron-angle counters which effectively subdivided the electron aperture into vertical slices for more precise definition of the electron-scattering angle and thus of the direction of the momentum transfer to the target proton.

Discrimination against negative pions was provided by a Freon-C-318-filled threshold Čerenkov counter and by a lead-Plexiglas shower counter. The background was sufficiently small that either of these counters used alone would have been sufficient to define electrons. In practice, the counters were adjusted to be 100% efficient for electrons during data taking. Small biases, reducing the electron-detection efficiency to between 95 and 98%, were introduced when the data were analyzed. With these biases, the pion contamination was negligible. Possible contamination by electrons from Dalitz decay of neutral pions was checked by reversing the spectrometer field and focusing positrons, since the decay gives rise to equal numbers of electrons and positrons. The contamination was found to be less than 1% and was ignored.

Since the energy of the scattered electron varies with the scattering angle, it was necessary to tilt the spectrometer counters in the horizontal plane to ensure the detection of electrons associated with a fixed pion-nucleon c.m. energy in a particular spectrometer energy bin. The tilt of the counters could be adjusted remotely between limits of 52° and 90° to the spectrometer axis.

C. Pion-Proton Coincidence Array

The pion-proton coincidence array consisted of a triple scintillator telescope, a 12×12 hodoscope, and a Plexiglas Čerenkov counter. The entire system was protected from low-energy, charged-particle background by a C magnet with 30 cm×30 cm pole pieces, 35 cm apart, positioned as close to the target as possible to maximize the solid angle subtended by the detectors. The solid angle subtended by the hodoscope in the present measurement was approximately 200 msr.

The data at 0.25 $(\mathrm{GeV}/c)^2$ were taken with an integrated clearing-field strength of 1.9 kG m. For the remainder of the measurements the field strength was 0.81 kG m. Reducing the field increased the background counting rate fractionally, but produced a significant reduction in the distortion of the coincidence particle trajectories caused by the clearing field.

The background counting rate was mainly target associated and depended strongly upon the adjustment of the magnets in the external electron beam and the angle of the coincidence arm with respect to the beam. Under the conditions of the present experiment the γ-ray background in the counters necessitated the use of a triple coincidence in order to reduce random coincidences to an acceptable level. Typically, with resolution time of 10 nsec, the triple coincidence rate $S_1S_2S_3$ was only 10% of the S_1S_2 coincidence rate.

In the majority of kinematic situations encountered in the experiment, pions from the $e^-+n+\pi^+$ final state had $\beta \gtrsim 0.9$, whereas protons from the π^0 reaction had $\beta \lesssim 0.7$. Therefore, in principle, a Plexiglas Čerenkov counter for which the threshold is $\beta \simeq 0.66$, provides a simple means of separating the two single-pion electroproduction reactions. Two such counters were constructed. The first was used in the measurement at 0.25 $(\mathrm{GeV}/c)^2$ and a second, improved version was used at all other four-momentum transfers except 0.6 $(\mathrm{GeV}/c)^2$, where both were employed.

IV. EXPERIMENTAL PROCEDURE

Whenever an event of interest occurred, an event pulse was generated. This pulse triggered a multiplexer circuit connected to the PDP-1 and initiated the transfer of the following information to the computer, where it was stored on magnetic tape.

(1) Pulse-height information from counters S_1 and S_2, the Plexiglas Čerenkov counter C, and the electron shower and Čerenkov counters.

(2) Information regarding which of the 35 electron counter and 24 hodoscope counter discriminators had been triggered.

(3) Pulse-height information from a time-to-amplitude converter (TAC) which registered the time difference between electron and coincidence-arm pulses.

(4) The incident beam energy at the time of the event.

(5) The presence of any of several real or delayed coincidences between selected counters.

(6) The current status of devices recording the integrated beam current, run time, and the total number of triggers which were presented to the computer.

An event pulse was generated by a fast triple coincidence $S_1S_2S_3$ in the recoil array in coincidence with either an "electron" pulse in the spectrometer, or an electron pulse delayed by approximately 42 nsec. The latter pulse was used to investigate the hodoscope distribution of random-coincidence events and was an essential feature of the experiment because the background flux was not uniform across the hodoscope. An event was labeled "real" or "delayed" by setting an appropriate bit in one of the multiplexer words.

An "electron" pulse was generated by the coincidence of at least two electron momentum counters, indicating the presence of a crossing trajectory in the quadrupole spectrometer, together with a pulse within the electron peak in the shower counter. The Freon Čerenkov counter was not involved in the formation of the event pulse.

The conditions necessary for the generation of an event pulse were deliberately kept nonselective in order to avoid the rejection of genuine events.

A. Scattered Electron Energy

The average energy focused in the central bin of the electron spectrometer as a function of the half-quadrupole current was determined experimentally by measuring the position of the elastic scattering peak for a large number of incident beam energies. In order to obtain a result which was independent of the angle of tilt of the spectrometer counters, a 1% correction was made to the scattered energy to obtain the energy which would have been focused at the pivot of the central counter with the same magnet current. This energy is independent of the counter tilt.

The calibration procedure was only used to obtain a curve of dE/di versus i, where E is the energy focused at the counter pivot and i is the current in the half-quadrupole magnet. The scattered energies for a particular set of electroproduction data were determined by first focusing the elastic-scattering peak at the center of the focal plane and then reducing the magnet current in order to focus the Δ peak. Since the scattered energy at the elastic peak was known, it was only necessary to use the magnet calibration to deduce the energy change produced by the change in current. This procedure led to an error of approximately ± 10 MeV in the pion-nucleon c.m. energy assigned to a particular spectrometer energy bin.

B. Calibration of Spectrometer Energy Bins

The acceptances of the nominally 1% wide energy bins of the electrons spectrometer were determined experimentally by letting each counter perform a stepwise integration over a particular electron energy spectrum. The incident electron energy and scattering angle were fixed and the current in the magnet was varied in equal steps in order to move the electron spectrum past the bin in question.

In the following discussion it is convenient to label quantities with two parameters, x the bin label and i the magnet current. The objective of the calibration was to determine $\Delta E(x,i_0)$, where $\Delta E(x,i_0)$ is the energy acceptance of the xth bin at current i_0, for all x.

Since the magnet did not saturate appreciably at the currents used,

$$\Delta E(x,i)=\Delta E(x,i_0)i/i_0$$

and

$$\frac{dE}{di}(x,i)=\frac{dE}{di}(0,i_0)(1+x)$$

with an accuracy better than 1%.

The formula for N_e, the total number of electrons in the particular spectrum, is

$$N_e=S_x\sum_{i_{\min}}^{i_{\max}}\left(\frac{dE/di(x,i)\Delta i}{\Delta E(x,i)}\right)N_i,$$

where the factor S_x corrects for the loss of electrons from the xth bin due to counter overefficiencies and inefficiencies, Δi is the current increment, and N_i is the number of counts obtained in the bin at current i. Substituting for dE/di and rearranging,

$$\Delta E(x,i_0)=\frac{S_x\Delta i i_0}{N_e}(1+x)\frac{dE}{di}(0,i_0)\sum_{i_{\min}}^{i_{\max}}\frac{N_i}{i}. \qquad (6)$$

Equation (6), without the factor $1/N_e$, gives the relative sizes of the energy bins. The absolute normalization of these bins was determined in two independent ways.

(1) For each fixed current, an energy interval centered on the peak was chosen. The nominal width of this interval was selected to be the same as that used in the determination of the relative bin sizes and an integral over the spectrum was performed using those counters which were within the interval. This integral, which determined N_e, was calculated for all currents which focused the peak of the spectrum sufficiently close to the center of the momentum counters that the complete energy interval was available.

(2) The second method of normalizing the bins was to move the elastic peak between two widely separated counters by a known change in current. However, the difficulty in determining the exact positions of the

elastic peak contributed a 2.5% error to the bin sizes in this method. In addition to the statistical errors and the error noted above, the measured bin widths contain uncertainties associated with instabilities in the energy and position of the electron beam. Fluctuations in the energy of the incident beam were kept below 0.02% and are estimated to contribute an error of less than 3% to the bin sizes. The low beam intensity used during the calibration measurements did not permit the horizontal position of the beam to be monitored with the rf cavity. Assuming the maximum horizontal fluctuations observed at higher beam intensities, the corresponding error in the bin widths is estimated to be 3%. The maximum vertical movement of the beam at the target is expected to be less than 0.1 mm, which contributes an additional error of less than 3.5%.

The errors due to these effects were minimized by varying the magnet current two increments at a time, with the intermediate steps filled in on a second pass across the spectrum. Adding the above errors in quadrature with the statistical errors, the over-all uncertainty in the width of a single energy bin is estimated to be 7%. This is the dominant source of systematic error in the present experiment.

C. Electron Scattering Angle

The electron scattering angle was measured by placing an accurately surveyed 3-mm glass slide in the electron beam. The spot produced on this slide and the beam position observed on the target tungstate screen served to determine the incident-beam direction and its position relative to the spectrometer aperture.

The rf cavity was used to monitor the beam position throughout the data taking and at the time of the glass-slide exposure. For some of the measurements the beam intensity was too low to produce a useful signal in the monitor. For these runs it was assumed that the angular deviations were as large as the maximum deviations observed in the runs for which rf cavity measurements were available.

The uncertainty in the scattering angle was estimated to be 0.5% at four-momentum transfers above 0.1 $(\mathrm{GeV}/c)^2$, giving rise to a 2% uncertainty in the cross section, due to the error in the factor Γ_T defined in Eq. (2). At $q^2=0.05$ $(\mathrm{GeV}/c)^2$, where the low beam intensity made beam monitoring difficult, the corresponding uncertainty in the cross section is 4%.

D. Beam-Intensity Limitations

Random coincidences between electrons and unassociated charged particles in the recoil arm were the principal source of background in the experiment. In order to ensure the reliability of the data, the beam intensity was reduced until the ratio of delayed to real events was approximately 0.1. Since the ratio of electrons with a coincidence to all electrons detected within the spectrometer was, typically, 0.1, the ratio of delayed coincidences to all electrons was 0.01.

If the delayed-to-real coincidence ratio had not limited the beam intensity, a similar problem, that of ambiguous hodoscope events, would have limited the beam to an intensity about twice as high as that which was actually used. At the beam intensities used, the probability of observing a random event in an additional hodoscope counter, in such a position that the genuine particle could not be located to within ± one bin, was 0.06.

V. DATA ANALYSIS

The analysis of the data was performed in three stages. In the first stage, the raw data stored on magnetic tape were analyzed for trajectories in the electron spectrometer which crossed the focal plane within the desired energy bin. Events satisfying the appropriate criteria were written by the PDP-1 computer onto a momentum-analyzed intermediate tape. At the second stage of the analysis the momentum-analyzed tape was reanalyzed with a second PDP-1 program. This program enabled biases to be introduced in the electron shower and Čerenkov counter spectra, and in counters S_1, S_2, and C of the coincidence arm in order to select genuine electrons, and pions or protons as required. The data from this stage were then used as input to an IBM 7094 computer program which performed three main tasks:

(1) tracing rays through the sweeping magnet in order to determine the angles and solid angles associated with each hodoscope bin,

(2) grouping of the hodoscope data into specified $\theta_\pi^*-\phi_\pi$ bins, and

(3) normalization and averaging of the hodoscope data associated with each electron-angle counter.

During the first stage of the analysis the computer not only assigned trajectories to the correct energy bins but, within each bin, sorted the events into several categories determined by the pattern of triggered counters. The events were first assigned to one of three general classifications:

(1) those events for which a falling electron trajectory crossing the focal plane of the spectrometer could be unambiguously identified,

(2) good, rising trajectories, and

(3) events which did not have a pattern characteristic of a crossing trajectory.

Events in classes (1) and (2) were further subdivided into ten categories, coded 00 through 22, and 77, where an error code *nl* indicates that the event has n counters missing from the perfect pattern and l extra counters on. Code 77 included all events with more than two counters inefficient or on in random coincidence.

The sum of categories 00 through 10 for rising and falling trajectories contained approximately 85% of all

event triggers and 95% of the eventually accepted events. Only these categories were written on to the momentum-analyzed tape and used to obtain the electroproduction angular distributions. The appropriate normalization factor for the cross section, S_x, was determined by hand-scanning a selection of several hundred events with higher error codes. The error in the correction factor is estimated to be less than 1.5%.

In order to extract the angular distributions as a function of pion-nucleon c.m. energy, the data were grouped into electron-energy bins which subtended approximately 2% of the scattered electron energy at four-momentum transfers of 0.05, 0.13, and 0.25 $(\mathrm{GeV}/c)^2$ and 1.5% at 0.4 and 0.6 $(\mathrm{GeV}/c)^2$. The corresponding interval in the π-N c.m. system was approximately 40 MeV. Since the cross section might be expected to vary rapidly with c.m. energy, the distorting effect of grouping the data into 40-MeV bins was examined using the dispersion theory of Adler.[24] For both π^0 and π^+ final states the errors introduced into the cross section were estimated to be less than 2% and were ignored.

The measurement of pion and proton angles was limited by an uncertainty of approximately 3° (lab) in the direction of the three-momentum transfer to the isobar system, due to the energy and angular resolution of the scattered electrons. In the analysis, the hodoscope data were grouped into large bins, which subtended horizontal and vertical laboratory angles at the target of approximately 6°. For positive pions the corresponding increment in c.m. polar angle was 8°–10°. For protons the increment was between 10° and 15°.

For small c.m. polar angles, i.e., in the direction of three-momentum transfer, the resolution did not permit a good measurement of ϕ_π. However, the azimuthal dependence of the cross section is small in this region and good resolution is not required. At large polar angles, the resolution was adequate and the data were grouped into ϕ_π bins 15°–25° wide.

A. Cross-Section Formula

The cross section associated with one (θ_π^*,ϕ_π) bin is given by a sum over all hodoscope (i,j) bins included within the angular bin, and over the electron-angle counters. The formula employed was

$$\frac{d^3\sigma(\bar{\theta}_e,\theta_\pi^*,\phi_\pi)}{d\Omega_\pi d\omega_e dE'} = \frac{1}{N_e N_p \Delta E' \alpha} \frac{\sum_{i,j}\sum_a [N(i,j)-N_r(i,j)f_r]u(i,j)}{\sum_{i,j}\sum_a [\Delta\Omega_{\pi,p}(i,j)\Delta\omega_e f_a]}, \quad (7)$$

where N_e is the number of incident electrons, N_p is the number of target protons per unit area normal to the incident beam, $\Delta E'$ is the width of electron energy bin, and α is a product of nine factors which correct the cross section normalization for

(1) combined efficiency of electron shower and Čerenkov counters,
(2) momentum analysis efficiency S_x,
(3) electron angle-counter efficiency,
(4) radiation by the electron,
(5) the computer dead time,
(6) the efficiency of the hodoscope counters,
(7) coincidence particle absorption,
(8) combined efficiency of S_1 and C for pion or proton detection, and
(9) empty target background.

$N(i,j)$ is the number of counts in the (i,j) hodoscope bin which survive all counter biases and for which the delay bit was off. $N_r(i,j)$ is the number of analyzed delayed events in the (i,j) bin. f_r is the correction factor to allow a large sample of delayed events to be used. (Since the angular distribution of delayed events did not depend on the electron momentum, a certain fraction of the total number of delayed events was subtracted from the counts associated with each electron momentum bin.)

f_a is the fraction of total electron counts observed in electron angle counter, a. $\Delta\Omega_{\pi,p}(i,j)$ is the c.m. π^+ (proton) solid angle. $\Delta\omega_e$ is the laboratory solid angle for electron detection. $u(i,j)$ is the pion decay correction = 1.0 for the π^0+p final state. For π^+ events, $u(i,j)$ varied between 1.0 and 1.12, depending upon the average pion momentum and the position of the bin within the hodoscope.

B. Radiative Corrections

In the region of the $\Delta(1236)$ resonance, the most important radiative correction is the Schwinger correction for electrons which are associated with the proper isobar energy W but which are detected at higher W (lower scattered energy) because of radiative energy loss by the scattered electron. If this were the only type of radiative correction, the experimentally observed doubly differential cross section would be related to the radiation-free cross section by

$$\left(\frac{d^2\sigma}{d\omega_e dE'}\right)_{\mathrm{expt}} = \frac{d^2\sigma}{d\omega_e dE'} e^{-\delta}, \quad (8)$$

where

$$\delta = \frac{2\alpha}{\pi}\left[\left(\ln\frac{E'}{\Delta E'}-\frac{13}{12}\right)\left(\ln\frac{q^2}{m^2}-1+\frac{\pi(t_a+t_b)}{\alpha \ln 2}\right)+\frac{17}{36}\right]$$

This formula includes the effect of physical radiators of thickness t_a radiation lengths after the target and t_b before it.[28] For the present measurement, $t_a = 0.009$ and $t_b = 0.003$.

[28] J. D. Bjorken, Ann. Phys. (N Y.) 24, 201 (1963).

Since the energies of the coincident pions or protons were not measured, only radiation from the electron was important. Therefore, no attempt was made to use a more complicated prescription for δ,[29] and Eq. (8) was assumed to hold for the triply differential cross section.

The other correction to the observed cross section is due to electrons which have radiated into the experimental energy bin from regions of lower W (higher E'). In the spirit of the "peaking approximation" it is assumed that this correction can be divided into radiation before and radiation after scattering.

In a notation similar to that of Bjorken,[28] the real and observed doubly differential cross sections are related by

$$\frac{d^2\sigma(\text{expt})}{d\omega_e dE'}(E,E',\theta_e)=\frac{d^2\sigma}{d\omega_e dE'}(E,E',\theta_e)e^{-\delta}+\int dE''P_b(E,E'')\frac{d^2\sigma}{d\omega_e dE'}(E'',E',\theta_e)+\int dE''\frac{d^2\sigma}{d\omega_e dE''}(E,E'',\theta_e)P_a(E'',E'), \quad (9)$$

where $P_b(E,E'')$ and $P_a(E'',E')$ are the probabilities for radiation before and after scattering, respectively,

$$P_{a,b}(E_1,E_2)\cong\frac{\alpha}{\pi}\frac{E_2}{(E_1-E_2)E_1}\times\left[\ln\frac{q^2}{m^2}-1+\frac{\pi t_{a,b}}{\alpha\ln 2}+\frac{(E_1-E_2)^2}{E_1E_2}\ln\frac{(E_1+E_2)}{m}\right]. \quad (10)$$

The P's are estimated to be reliable to within 20%.

The corrections to the triply differential cross sections were performed using a prescription similar to that of Eq. (9). In order to avoid the problem of calculating the efficiency for detecting coincident particles as a function of W, experimentally observed cross sections were used in the radiation integrals. Since the observed cross sections were not corrected for radiation, an iterative procedure was used.

In the first iteration, the cross sections in the second integral were replaced by the cross sections obtained experimentally at each value of E''. The cross sections in the first integral were approximated by multiplying the observed cross sections by a factor to correct for the kinematic and form factor variations, produced by the changes in the electron energies. Specifically, the approximation used was

$$\frac{d^3\sigma}{d\omega_e dE' d\Omega_\pi}(E_1,E_2,\theta_e,\Omega_\pi)=\frac{\Gamma_T(E_1,E_2)}{\Gamma_T(E_3,E_4)}\frac{F(E_1,E_2)}{F(E_3,E_4)}\frac{d^3\sigma(\text{expt})}{d\omega_e dE' d\Omega_\pi}(E_3,E_4,\theta_e,\Omega_\pi) \quad (11)$$

[29] P. Urban and F. Widder, Institute for Theoretical Physics, University of Graz, Austria, Report, 1966 (unpublished).

at fixed W and E_3, so that only two of E_{1-4} are independent. Γ_T is the kinematic factor defined in Eq. (2) and F is a factor describing the dynamics of the photon-hadron vertex. F was approximated by the magnetic dipole contribution to the cross section[22]

$$F=\mathbf{q}^{*2}/(1+q^2/0.71)^4.$$

The iteration was continued until successive values of the corrected cross section differed by less than 1%.

Since radiation into the energy bin from radiation before scattering was approximately 5% of the observed cross section, an error of 40% in the radiation integral contributes 2% uncertainty to the over-all correction. This is of the same order as the uncertainty connected with the peaking approximation. The over-all uncertainty in the radiative correction is extremely difficult to estimate reliably. However, it is expected to be less than 4%.

C. Pion-Proton Separation

The separation of positive pions from protons was achieved by setting biases in the pulse height spectra of counters S_1, S_2, and C. Figure 4 shows the S_1 spectrum at $q^2=0.13$ (GeV/c)^2, $W=1.23$ GeV, where the pion and proton peaks were well separated. In this region it was possible to isolate a sample of pions with negligible proton contamination by placing biases in the S_1 and C pulse-height spectra to produce an over-all detection efficiency of about 80%. Similarly, pure samples of protons could be isolated with an efficiency of about 98%.

The angular distributions presented in this paper were determined only from the events which survived the biases in S_1 and C. The absolute normalization was determined as follows. Biases were set in two counters at a time and the resulting pion or proton spectrum in the third counter was examined to determine its efficiency. This was done with several biases until the pure pion and proton spectra were known in each of the three

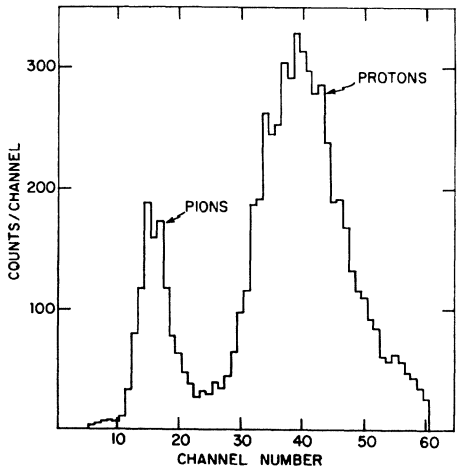

FIG. 4. Pulse-height spectrum in counter S_1. $q^2=0.130$ (GeV/c)^2; $W=1226$ MeV.

counters. The efficiency for the S_1-C bias could then be obtained by estimating the total number of pions or protons in either S_1 or C before setting the bias and comparing this number with the number of events surviving the biases. Alternatively, since the spectra in S_1 and C were uncorrelated, the efficiency could also be calculated as the product of the efficiencies in each counter. The results using each of the above procedures were consistent.

At four-momentum transfers above 0.3 $(\mathrm{GeV}/c)^2$ the specific ionizations of the pions and protons became similar and the separation was more difficult. In this case, the detection efficiency for the less common π^+ events was often reduced to 50–70% in order to prevent proton contamination and was more difficult to estimate. The procedure was complicated by the strong correlation between pulse heights in S_1 and S_2, and the absorption of pions between S_3 and C. However, the efficiency was estimated in several ways for each set of biases and agreement to within 5% was obtained in all cases.

D. Hodoscope Analysis

The calculation of the solid angle associated with each of the hodoscope bins was complicated by the presence of the sweeping magnet field. Because the field was nonuniform it was necessary to make detailed measurements of the field and to employ a computer program to trace the particle trajectories from the target to the hodoscope. All three components of the magnetic field were measured with a Hall probe with a reproducibility of about 0.2%.

The computer program used to do the ray tracing was an adaption of a CERN program.[30] The solid angle subtended by each hodoscope bin was determined by finding the rays from the target center which passed through the four corners of the bin. An initial set of trial rays were chosen using an effective-length model for the sweeping magnet and the final rays were obtained by iteration.

The uncertainties in the laboratory solid angles are estimated to be less than 2.5% for all except the measurements at 0.25 $(\mathrm{GeV}/c)^2$, where they are expected to be approximately 3.0%. The uncertainty is primarily due to the fact that the nonuniform particle deflection results in a distortion of the rectangular bin shapes. The net deflection of the particles varied between 3 and 9 cm at the hodoscope and was usually no larger than the horizontal dimensions of the composite bins chosen for grouping the data.

E. Backward Protons in the Reaction $e^-+p\rightarrow e^-+p+\pi^0$

Protons from the reaction $e^-+p\rightarrow e^-+p+\pi^0$ emerge within a cone of semivertical angle α about the direction of the three-momentum transfer, where $\alpha=\mathfrak{L}\theta^*_m$ and $\cos\theta^*_{\max}=-|\mathbf{p}^*|/\beta_c p_0^*$. Here $\mathfrak{L}$ is the Lorentz transformation connecting the proton lab angle to the corresponding c.m. angle, β_c is the velocity of the pion-nucleon system in the lab, and $\mathbf{p}^*$ and p_0^* are the momentum and energy of the proton in the c.m. system.

For laboratory angles less than α, two groups of protons are observed, one with $\theta^*>\theta^*_m$, the other with $\theta^*<\theta^*_m$. In the following discussion, the former will be called backward protons, the latter forward.

The energies of the two groups of protons differ considerably, with the exception of a small angular region near θ^*_m and, for the majority of four-momentum transfers, the backward protons were stopped before they could be counted in the hodoscope. No attempt was made to evaluate forward proton cross sections from hodoscope bins where there was any possibility of backward proton contamination. In practice, except for the measurement at 0.6 $(\mathrm{GeV}/c)^2$, where the range of backward protons was sufficient to contaminate the whole hodoscope, this limitation merely meant restricting the maximum proton lab angle to approximately 15°. At 0.6 $(\mathrm{GeV}/c)^2$ the analysis was confined to π^+ cross sections.

VI. NONCOINCIDENCE CROSS SECTIONS

At frequent intervals during the course of the inelastic coincidence runs, measurements of the elastic cross section were made in order to provide a check of the inelastic cross-section normalization. Since the recoil protons from elastic electron scattering were outside the angular acceptance of the coincidence array, the elastic cross sections were measured by detecting the scattered electron alone.

The data were analyzed in a manner similar to that described by Goitein *et al.*[25] The results are shown in Fig. 5, where they are plotted as ratios to the cross sections predicted by the Rosenbluth formula with the

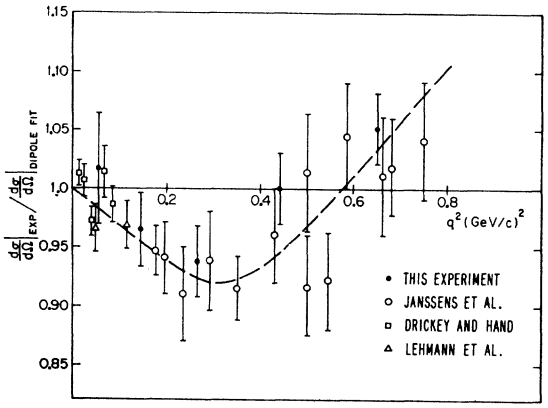

FIG. 5. Elastic electron-proton differential cross-section measurements expressed as ratios to the dipole fit cross section. The dashed line serves only to guide the eye.

[30] L. Griffiths, C. R. Symons, and B. Zacharov, CERN Report No. 66-17, 1966 (unpublished). We are grateful to L. Griffiths for providing us with a FORTRAN listing of this program and invaluable explanatory comments.

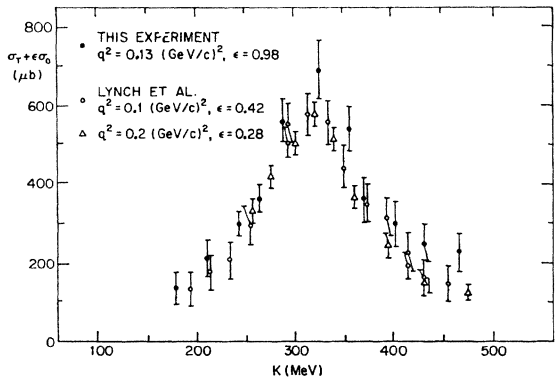

FIG. 6. Noncoincidence inelastic electron-proton scattering. $(d^2\sigma/dE'd\Omega)/\Gamma_T$ as a function of the equivalent photon energy at four-momentum transfers between 0.1 and 0.2 (BeV/c)^2.

proton form factors assumed to obey the scaling law and the dipole fit[31]

$$G_{Mp}/\mu_p = G_{Ep} = [1+q^2/0.71\ (\mathrm{GeV}/c)^2]^{-2}. \quad (12)$$

Also shown in the figure are some previous measurements in this region of four-momentum transfer.[32–34] The agreement is satisfactory. The dashed line serves only to indicate the general trend of the data and has no other significance.

The observed cross sections depart systematically from the predictions of the dipole fit and the scaling law. The most important effect of this involves the comparison of the inelastic coincidence cross sections with the dispersion-theory predictions of Adler and of Zagury. These theories were evaluated with the dipole fit form factors. Because of this, and the similar four-momentum transfer dependence of elastic and inelastic scattering, the predictions of Adler and of Zagury for π^0 production have been multiplied by the ratio of the elastic cross sections to those predicted by the dipole fit. In the π^+ production, the theoretical predictions were not normalized in this way because of the dominance of the pion form factor, which was treated as a free parameter.

The elastic-scattering cross-section values and the ratios to the dipole-fit predictions are shown in Table II.

A further check on the over-all normalization of the cross section is provided by comparing measurements of the doubly differential inelastic cross section, obtained by detecting the scattered electron alone, with previous measurements. Figure 6 shows a comparison of data obtained at a four-momentum transfer near 0.13 (GeV/c)^2 with the measurements of Lynch *et al.*[3] at $q^2=0.1$ and 0.2 (GeV/c)^2. The present measurements are also listed in Table III. For the purpose of comparison the cross sections have been normalized by dividing by Γ_T. The agreement is generally good.

VII. DIFFERENTIAL CROSS SECTIONS FOR π^0 ELECTROPRODUCTION

Figures 7–10 show π^0 angular distributions plotted as a function of ϕ_π for several representative pion-nucleon c.m. energies at four-momentum transfers of 0.05, 0.13, 0.24, and 0.4 (GeV/c)^2. The solid and dashed lines are the theories of Adler and of Zagury, respectively, normalized as discussed in Sec. VI. This change in normalization was less than 6% in all cases (see Fig. 5).

The over-all agreement between theory and experiment is remarkably good, but several general trends can be identified.

(1) The agreement is best in the region of the resonance peak, especially below $q^2=0.4$ (GeV/c)^2 (Figs. 7–9).

(2) The theories underestimate the differential cross sections for W greater than the resonance energy (Fig. 9). Zagury's theory[12] is somewhat better in this

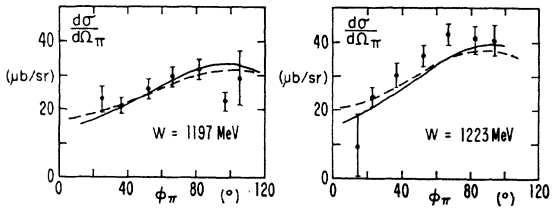

FIG. 7. Azimuthal angular distributions for the reaction $e^-+p\rightarrow e^-+p+\pi^0$ at $q^2\simeq 0.05$ (GeV/c)^2, $\theta_\pi^*=130°$ for two different pion nucleon c.m. energies. The solid and dashed lines are the predictions of Adler and of Zagury, respetcively.

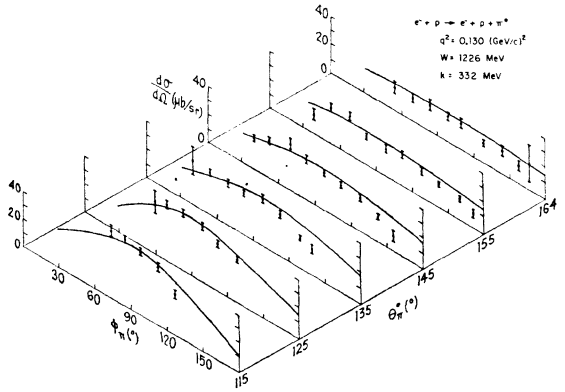

FIG. 8. Angular distributions for the reaction $e^-+p\rightarrow e^-+p+\pi^0$ compared with Adler's theory at $q^2=0.130$ (GeV/c)^2, $W=1226$ MeV. The effect of the small cosϕ term in the measured cross section, which tends to depress the data relative to the theory for $\phi>90°$ and enhance it for $\phi<90°$, is visible at most pion polar angles.

[31] M. Goitein, J. R. Dunning, Jr., and Richard Wilson, Phys. Rev. Letters **18**, 1018 (1967).
[32] D. J. Drickey and L. N. Hand, Phys. Rev. Letters **9**, 521 (1962).
[33] P. Lehmann, R. Taylor, and Richard Wilson, Phys. Rev. **126**, 1183 (1962).
[34] T. Janssens, R. Hofstadter, E. B. Hughes, and M. R. Yearian, Phys. Rev. **142**, 922 (1966).

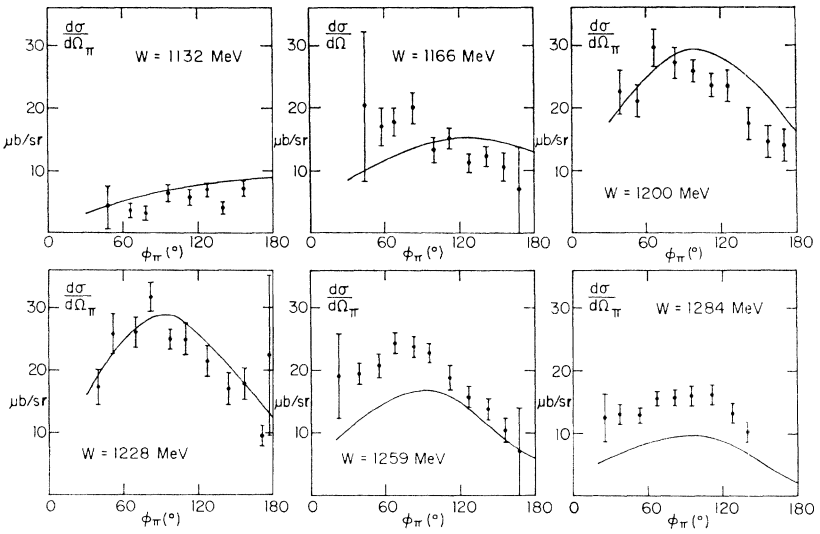

FIG. 9. Azimuthal angular distributions for the reaction $e^-+p\rightarrow e^-+p+\pi^0$ compared with Adler's theory at $q^2\simeq 0.25$ (GeV/c)^2, $\theta_\pi^*=135°$ for several pion-nucleon c.m. energies.

respect. However, a comparison of Adler's[24] theory with Lynch's *total cross-section* data[3] indicates no such discrepancy in this region of four-momentum transfer. The underestimation could be due to an angular distribution effect which tends to cancel in other regions of θ_π^*. However, a comparison of Adler's theory with the total cross-section data of Cone *et al.*[35] at $q^2=1$ (GeV/c)^2 and above indicates that the theory is too low above the resonance. Once again, Zagury's theory fits the data better.

(3) The theories underestimate the π^0 cross section for $\theta_\pi^*>90°$ at $q^2=0.4$ (GeV/c)^2, even at the resonance energy (Fig. 10). Since the theories fit the total cross-section data at higher four-momentum transfers, this is probably also due to errors in the calculation of the π^0 angular distribution. It is well known that the theories do not agree with backward angle π^0 photoproduction measurements. However, in the latter case the theories *overestimate* the cross section.

There are π^0 coincidence data[6] from the Deutsches Elektronen Synchrotron (DESY) at $q^2=0.8$ (GeV/c)^2 which are generally higher than theory and tend to substantiate the present measurements at 0.4 (GeV/c)^2.

(4) Although the π^0 azimuthal distributions are dominated by the large $\cos 2\phi_\pi$ term, as predicted, there is also evidence for a significant scalar-transverse ($\cos\phi_\pi$) interference term at $q^2=0.13$ and 0.25 (GeV/c)^2 (Figs. 8 and 9).

Two other π^0 coincidence experiments have suggested the presence of scalar interactions. Measurements were made at the Tokyo synchrotron[7] at $q^2=0.12$ (GeV/c)^2. The 180° π^0 cross section, obtained for $\epsilon=0.5$ and 0.7,

TABLE II. Electron-proton elastic scattering cross-section values.

q^2 (GeV/c)^2	E (GeV)	θ_e (°)	$d\sigma/d\omega_e$ (cm^2/sr)	Ratio to dipole-fit prediction
0.055	2.001	6.77	$(8.72\pm0.41)\times10^{-29}$	1.017±0.047
0.145	3.264	6.76	$(2.27\pm0.07)\times10^{-29}$	0.965±0.031
0.267	4.517	6.67	$(8.30\pm0.27)\times10^{-30}$	0.938±0.030
0.422	4.529	8.64	$(1.89\pm0.06)\times10^{-30}$	1.003±0.031
0.650	5.019	9.55	$(6.42\pm0.20)\times10^{-31}$	1.051±0.033

TABLE III. Noncoincidence inelastic electron scattering from hydrogen. $(d^2\sigma/dE'd\omega_e)/\Gamma_T$ as a function of the equivalent photon energy at a four-momentum transfer near 0.13 (GeV/c)^2. $E=3.264$ GeV; $\theta_e=6.76°$.

K (GeV)	$\sigma_T+\epsilon\sigma_0$ (μb)	Error (μb)
0.179	137	28
0.211	215	44
0.242	300	47
0.264	364	40
0.288	567	61
0.325	699	76
0.356	545	85
0.387	355	72
0.406	259	53
0.431	250	51
0.467	226	46

[35] A. A. Cone, K. W. Chen, J. R. Dunning, Jr., G. Hartwig, N. F. Ramsey, J. K. Walker, and Richard Wilson, Phys. Rev. **156**, 1490 (1967).

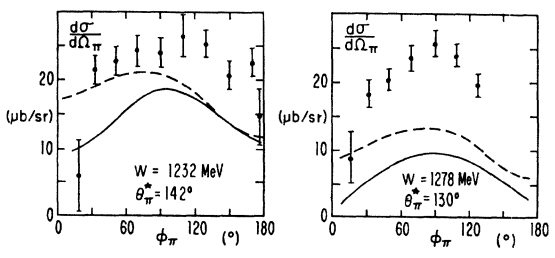

FIG. 10. Azimuthal angular distributions for the reaction $^-+p\rightarrow e^-+p+\pi^0$ at $q^2\simeq 0.4$ (GeV/c)^2. The solid and dashed enes are the predictions of Adler and of Zagury, respectively.

indicated a large scalar term, but with rather large errors. The DESY data[6] at $q^2=0.8$ (GeV/c)^2, $\theta_\pi{}^*=90°$, taken at two different electron angles, also showed evidence for a scalar term, but again the errors were large.

(5) At $q^2=0.13$ (GeV/c)^2, $K=276$ MeV, the present π^0 data lie below the theoretical predictions by almost a factor of 2. This is surprising in view of the good agreement at $K=332$ MeV for the same four-momentum transfer and at similar K values at $q^2=0.05$ and 0.25 (GeV/c)^2. Normalization errors have been searched for but have not been found.

A. Phenomenological Analysis of the π^0 Data

For the π^0 process, which does not have large contributions from the pion pole term, it is possible to describe the cross section in terms of a multipole expansion including only S and P pion-nucleon partial waves. In this section a multipole expansion is presented for each part of the cross section described in Sec. II C. However, since a fit to the data in terms of multipoles requires a large number of parameters, the cross section has been described in terms of six parameters which characterize the only possible angular dependence consistent with the presence of S and P waves. The fits to the data using these parameters should give some insight into the more fundamental multipole information and will serve as a useful starting point for a more complete analysis of the data.

The electroproduction cross section can be described in terms of six independent amplitudes, F_i ($i=1$ to 6).[22] For the purpose of separating the scalar and transverse contributions it is common practice to work with F_1 through F_4 which are purely transverse and two purely scalar, linear combinations of the original six, F_7 and F_8. In terms of these, the various terms of Eq. (5) can be written as[36]

$$\begin{aligned}
d\sigma_T/d\Omega_\pi &= (|\bar{\pi}^*|W/MK)[|F_1|^2+|F_2|^2 \\
&\quad -2\cos\theta_\pi{}^*\,\mathrm{Re}(F_1)(F_2)^*]+\sin^2\theta_\pi{}^*\,T(\theta_\pi{}^*), \\
d\sigma_0/d\Omega_\pi &= (|\bar{\pi}^*|W/MK)(q^2/\mathbf{q}^{*2}) \\
&\quad \times[|F_7|^2+|F_8|^2+2\cos\theta_\pi{}^*\,\mathrm{Re}(F_7)(F_8)^*], \\
T(\theta_\pi{}^*) &= (|\bar{\pi}^*|W/2MK)[|F_3|^2+|F_4|^2 \\
&\quad +2\,\mathrm{Re}(F_2F_3{}^*+F_1F_4{}^*+F_3F_4{}^*\cos\theta_\pi{}^*)], \\
S(\theta_\pi{}^*) &= -(2|\bar{\pi}^*|W/MK)(q^2/\mathbf{q}^{*2})^{1/2}\,\mathrm{Re}[(F_1+F_4 \\
&\quad +F_3\cos\theta_\pi{}^*)F_7{}^*+(F_2+F_3+F_4\cos\theta_\pi{}^*)F_8{}^*]. \qquad (13)
\end{aligned}$$

The multipole expansions of the F's are given by Zagury.[12] The P-wave scalar multipole $S_1{}^+$ appears in this expansion via the equations

$$\begin{aligned}
F_7 &= \sum_l (S_l{}^- - S_l{}^+)P_l'(\cos\theta_\pi{}^*), \\
F_8 &= \sum S_l{}^+P_{l+1}'(\cos\theta_\pi{}^*) - S_l{}^-P_{l-1}'(\cos\theta_\pi{}^*),
\end{aligned} \qquad (14)$$

and is defined to be twice as large as the $S_1{}^+$ of Adler[24] and others. Including only S and P waves leaves seven possible multipoles, giving

$$\begin{aligned}
F_1 &= E_0{}^+ + 3\cos\theta_\pi{}^*\,(M_1{}^+ + E_1{}^+), \\
F_2 &= 2M_1{}^+ + M_1{}^-, \\
F_3 &= 3(E_1{}^+ - M_1{}^+), \\
F_4 &= 0, \\
F_7 &= S_1{}^- - S_1{}^+, \\
F_8 &= S_0{}^+ S_1{}^+ \times 3\cos\theta_\pi{}^*.
\end{aligned} \qquad (15)$$

Substituting for the F's in Eq. (13) and rearranging, the cross section may be written as

$$\begin{aligned}
d\sigma/d\Omega_\pi &= A + B\cos\theta_\pi{}^* + C\cos^2\theta_\pi{}^* \\
&\quad + (D + E\cos\theta_\pi{}^*)\sin\theta_\pi{}^*\cos\phi_\pi \\
&\quad + F\sin^2\theta_\pi{}^*\cos 2\phi_\pi, \qquad (16)
\end{aligned}$$

where the multipole expressions for the coefficients A through F are

$$\begin{aligned}
A &= (|\bar{\pi}^*|W/MK)\{|E_0{}^+|^2+\tfrac{5}{2}|M_1{}^+|^2+\tfrac{9}{2}|E_1{}^+|^2 \\
&\quad +|M_1{}^-|^2-\mathrm{Re}[(M_1{}^-)(M_1{}^+)^*+3E_1{}^+(M_1{}^+-M_1{}^-)^*] \\
&\quad +\epsilon(q^2/\mathbf{q}^{*2})[|S_1{}^-|^2+|S_1{}^+|^2+|S_0{}^+|^2 \\
&\quad -2\,\mathrm{Re}(S_1{}^-)(S_1{}^+)^*]\}, \\
B &= (2|\bar{\pi}^*|W/MK)\,\mathrm{Re}\{E_0{}^+(M_1{}^+-M_1{}^-+3E_1{}^+)^* \\
&\quad +\epsilon(q^2/\mathbf{q}^{*2})[S_0{}^+(2S_1{}^+ + S_1{}^-)^*]\}, \\
C &= (|\bar{\pi}^*|W/MK)\{-\tfrac{3}{2}|M_1{}^+|^2+\tfrac{9}{2}|E_1{}^+|^2 \\
&\quad +3\,\mathrm{Re}[M_1{}^+(3E_1{}^+-M_1{}^-)^*-3M_1{}^-(E_1{}^+)^*] \\
&\quad +\epsilon(3q^2/\mathbf{q}^{*2})[|S_1{}^+|^2+2\,\mathrm{Re}S_1{}^+(S_1{}^-)^*]\}, \\
D &= -(2|\bar{\pi}^*|W/MK)(q^2/\mathbf{q}^{*2})^{1/2}\,\mathrm{Re}[E_0{}^+(S_1{}^- - S_1{}^+)^* \\
&\quad +S_0{}^+(3E_1{}^+ + M_1{}^- - M_1{}^+)^*][\tfrac{1}{2}\epsilon(\epsilon+1)]^{1/2}, \\
E &= -(6|\bar{\pi}^*|W/MK)(q^2/\mathbf{q}^{*2})^{1/2}\,\mathrm{Re}[E_1{}^+(2S_1{}^- + S_1{}^+)^* \\
&\quad +S_1{}^+(M_1{}^- - M_1{}^+)^*][\tfrac{1}{2}\epsilon(\epsilon+1)]^{1/2}, \\
F &= \epsilon(|\bar{\pi}^*|W/2MK)\{9|E_1{}^+|^2-3|M_1{}^+|^2 \\
&\quad -6\,\mathrm{Re}[E_1{}^+(M_1{}^+)^*+M_1{}^-(M_1{}^+-E_1{}^+)^*]\}. \qquad (17)
\end{aligned}$$

A least-squares fit to the neutral pion data was performed with A through F as free parameters. The analysis provided four major results.

(1) The data can be adequately described in terms of S and P partial-wave amplitudes.

(2) There are significant scalar-transverse ($\cos\phi_\pi$) terms in the cross section at $q^2=0.13$ and 0.25 (GeV/c)^2, which are most simply interpreted as interference between the $S_1{}^+$ (scalar quadrupole) and $M_1{}^+$, magnetic dipole, partial-wave amplitudes.

(3) The electric quadrupole $E_1{}^+$ amplitude is typically 5–13% of the resonant $M_1{}^+$ magnetic dipole amplitude, in reasonable agreement with photoproduction analyses.[37]

[36] N. Zagury, Nuovo Cimento **52**, 506 (1967); the term W_3 in this paper should be replaced by $-2W_3$; S. Adler and N. Zagury (private communication).

[37] F. A. Berends, A. Donnachie, and D. L. Weaver, Nucl. Phys. **B4**, 165 (1967).

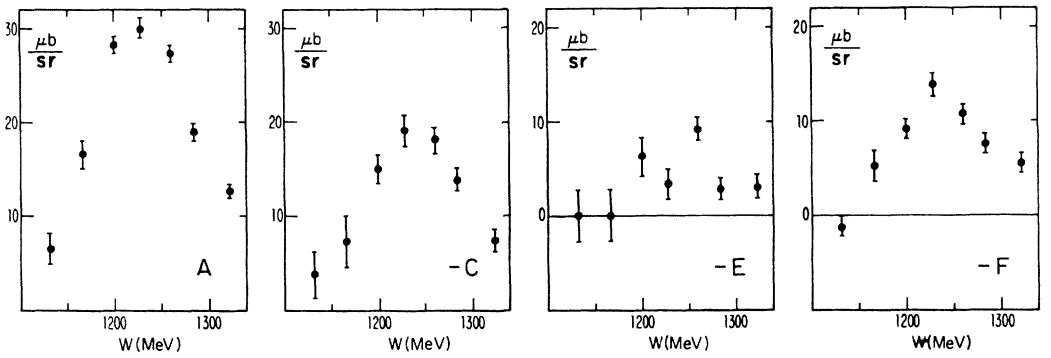

FIG. 11. Phenomenological analysis of the reaction $e^-+p \rightarrow e^-+p+\pi^0$. Best-fit angular coefficients at $q^2 \simeq 0.25$ (GeV/c)^2.

(4) The four-momentum transfer dependence of the M_1^+ amplitude, which is often described as the $\gamma N\Delta$ transition form factor, is approximately proportional to the nucleon isovector magnetic form factor, as suggested by Ash *et al.*,[38] but is also consistent with the exponential form-factor dependence proposed by Dufner and Tsai.[39]

Since neutral pion production in this energy region is known to be dominated by the magnetic dipole amplitude M_1^+, examination of the expressions for the angular coefficients shows that A, C, and F will be the dominant terms in the cross section. Furthermore, if the other multipole amplitudes are sufficiently small, the three coefficients will be related by $-\frac{3}{5}A=C=F/\epsilon$.

For each data set at fixed W, q^2, and ϵ, the results were fitted with the expression given by Eq. (16) with A through F as free parameters. In all cases the minimum values of χ^2 were reasonably consistent with the assumption that only S and P waves were present. For five of the 14 data sets, it was possible to obtain three-parameter fits in A, C, and F which represented the data well and which could not be improved significantly by adding extra free parameters. However, in no case was the relation $-\frac{3}{5}A=C=F/\epsilon$ obeyed within the errors, indicating the presence of significant interference terms in the cross section.

For the remaining data sets, four-parameter fits with either D or E as the additional parameter produced a reduction in χ^2, implying the presence of scalar-transverse interference terms in the cross section. However, the two alternative fits which were obtained for each data set were essentially identical, since in every case A, C, and F were unchanged within their errors, while the best-fit values of D and E were related by $D \simeq -0.7E$. When five-parameter fits were performed with both D and E as free variables, χ^2 remained essentially constant, but the best-fit values of D and E became unstable. Measurements with improved precision over a wider range of pion polar angles will be necessary to determine D and E on a purely phenomenological basis.

There are, however, physical grounds which indicate that the fits involving A, C, E, and F are to be preferred. The leading term in D is expected to be $\mathrm{Re}(S_0^+)(M_1^+)^*$, which will pass through zero in the vicinity of the resonance (since the phase of S_0^+ is small) while E contains the term $\mathrm{Re}(S_1^+)(M_1^+)^*$, which should peak at the resonance. Figure 11 shows the behavior of the fitted parameters at $q^2=0.25$ (GeV/c)^2 as a function of pion-nucleon c.m. energy. The fact that the coefficient of the $\cos\phi_\pi$ term remains positive across the resonance would appear to rule out the S_0^+, M_1^+ interference term as the dominant contribution. Therefore, although the situation may be considerably more complicated, the simplest interpretation of the data is that a major part of the observed scalar-traverse interference term is due to the resonant S_1^+ multipole amplitude and that the size of the S_1^+ amplitude is roughly consistent with the threshold relation

$$S_1^+/E_1^+=2|\mathbf{q}^*|/q_0^*.$$

Although the unambiguous definition of the leading scalar multipoles is difficult because of the problems outlined above, the precision with which the parameters A, C, and F have been determined, and their stability under the inclusion of the $\cos\phi_\pi$ term in the fits, enable more definite statements to be made about the transverse multipoles.

If it is assumed that the scalar-transverse interference term is caused by S_1^+, M_1^+ interference, the contribution to A and C from the $|S_1^+|^2$ term is probably no more than 5% in the worst case. However, because of their small phases, the S_0^+ and the S_1^- amplitudes could conceivably make large contributions to A, even though they give rise to small interference terms. No such problems can occur in C. For this reason C and F have been used to calculate values of $\mathrm{Re}(E_1^+)(M_1^+)^*$ and $|M_1^+|^2$. Since both C and F contain the expression

$$\tfrac{9}{2}|E_1^+|^2-\tfrac{3}{2}|M_1^+|^2-3\,\mathrm{Re}(M_1^-)(M_1^+)^*, \quad (18)$$

[38] W. W. Ash, K. Berkelman, C. A. Lichtenstein, A. Ramanauskas, and R. H. Siemans, Phys. Letters **24B**, 165 (1967).
[39] A. J. Dufner and Y. S. Tasi, Phys. Rev. **168**, 1801 (1968).

TABLE IV. Best-fit phenomenological parameters for neutral-pion electroproduction.

q^2 (GeV/c)^2	W (GeV)	ϵ	A (μb/sr)	$-C$ (μb/sr)	E (μb/sr)	F (μb/sr)	No. of datum points	χ^2	H_{AC}	H_{AF}	H_{CF}
0.0463	1.223	0.974	49.3±2.6	40.0±3.6	···	−20.4±2.8	32	22.3	− 8.9	1.5	−1.7
0.0475	1.197	0.978	34.4±2.3	22.1±3.1	···	− 8.4±2.7	41	58.1	− 7.0	2.6	−2.6
0.127	1.270	0.982	25.2±2.3	17.9±2.7	−9.7±2.7	−18.3±2.7	58	53.2	− 6.2	5.8	−6.4
0.130	1.226	0.984	29.3±2.1	13.1±2.6	−7.8±2.1	−21.8±2.5	55	54.0	− 5.2	4.8	−5.3
0.132	1.182	0.987	10.6±0.6	0.1±1.1	···	− 7.0±0.7	49	77.7	0.5	0.2	−0.2
0.240	1.321	0.984	12.7±0.8	7.5±1.1	−3.0±1.2	− 5.5±1.0	63	63.7	− 0.8	0.5	−0.6
0.243	1.284	0.985	19.0±0.8	13.8±1.2	−2.8±1.1	− 7.5±1.0	61	80.0	− 0.9	0.6	−0.6
0.245	1.259	0.986	27.4±0.9	18.1±1.4	−9.2±1.2	−10.7±1.1	66	52.2	− 1.2	0.6	−0.6
0.247	1.228	0.987	30.0±1.0	19.1±1.7	−3.4±1.7	−13.8±1.3	59	48.0	− 1.5	0.5	−0.4
0.250	1.200	0.988	28.4±0.9	15.0±1.5	−6.5±1.8	− 9.1±1.0	60	47.7	− 1.1	0.3	−0.1
0.252	1.166	0.989	16.6±1.5	7.3±2.8	···	− 5.3±1.5	35	25.1	− 4.0	0.7	−0.6
0.255	1.132	0.990	7.1±1.1	3.7±2.4	···	1.3±1.0	26	23.8	− 2.6	0.3	−0.1
0.398	1.278	0.978	24.8±1.5	17.8±2.0	−3.1±1.3	−11.2±1.8	31	24.3	− 3.0	1.5	−1.8
0.404	1.232	0.980	39.3±3.2	26.9±4.3	2.6±2.1	−11.0±3.1	26	44.7	−13.5	−0.2	−0.6

it is possible to obtain the equation

$$(|\bar{\pi}^*|W/MK)\,\mathrm{Re}(E_1^+)(M_1^+)^*=\tfrac{1}{12}(C-F/\epsilon) \quad (19)$$

by assuming only that $\mathrm{Re}(E_1^+)(M_1^+)^*\gg\mathrm{Re}(E_1^+)(M_1^-)^*$ and that the scalar terms in C are negligible. The additional assumption that $3|E_1^+|^2\ll|M_1^+|^2$ leads to the expression

$$|M_1^+|^2\left[1+\frac{2\,\mathrm{Re}(M_1^-)(M_1^+)^*}{|M_1^+|^2}\right]=-\tfrac{1}{6}\left(C+\frac{3F}{\epsilon}\right). \quad (20)$$

The ratio $\mathrm{Re}(M_1^-)(M_1^+)/M_1^{+2}$ at $q^2=0$ can be obtained from the analysis of Ref. 37. At the highest and lowest four-momentum transfers the use of this value led to a variation of M_1^+ across the resonance which was consistent with the behavior expected on the basis of the pion-nucleon phase shifts.[40] However, at the two intermediate four-momentum transfer points, a more consistent behavior for M_1^+ was obtained when no correction for this term was made. Because of this we have arbitrarily used one-half of the $q^2=0$ correction at all four-momentum transfers and assigned an appropriately large uncertainty to the value of M_1^+ obtained from Eq. (20). The correction to M_1^+ was 0% at resonance and, typically, 15% elsewhere.

TABLE V. Multipole amplitudes in the reaction $e^-+p\to e^-+p+\pi_0$. The quantities $|M_1^+|^2$ and $\mathrm{Re}(E_1^+)(M_1^+)^*$ were derived from the phenomenological parameters C amd F.

q^2 (GeV/c)^2	W (GeV)	$(\bar{\pi}W/MK)\,\lvert M1^+\rvert^2$ (μb/sr)	$\mathrm{Re}(E1^+)(M1^+)^*/\lvert M1^+\rvert^2$
0.0463	1.223	17.4 ±2.4	−0.09±0.03
0.0475	1.197	9.1 ±2.0	−0.12±0.05
0.127	1.270	10.7 ±1.8	+0.01±0.04
0.130	1.226	13.3 ±1.6	+0.06±0.03
0.132	1.183	4.56±1.3	+0.13±0.05
0.240	1.321	3.19±1.0	−0.05±0.05
0.243	1.284	5.14±1.2	−0.10±0.04
0.245	1.259	7.37±1.4	−0.08±0.03
0.247	1.228	10.1 ±1.2	−0.04±0.02
0.250	1.200	8.0 ±1.4	−0.06±0.02
0.252	1.166	5.9 ±2.1	−0.03±0.05
0.398	1.278	7.4 ±1.6	−0.07±0.04
0.404	1.232	9.8 ±2.0	−0.13±0.05

The best phenomenological fits to the data are shown in Table IV. The errors given for the fitting parameters are statistical only. The quantities $H_{\alpha\beta}$ are the correlation coefficients among A, C, and F. The values obtained for $|M_1^+|^2$ and $\mathrm{Re}(M_1^+)(E_1^+)^*/|M_1^+|^2$ are given in Table V. The errors are estimated standard deviations and include all sources of statistical, normalization and theoretical errors. In all cases, the ratio $\mathrm{Re}(M_1^+)(E_1^+)^*/|M_1^+|^2$ is small, in agreement with photoproduction results. The sign of the interference is negative at the lowest four-momentum transfer value, as it is in photoproduction, but becomes positive at $q^2=0.13$ (GeV/c)^2, and finally becomes negative again.

It is interesting to note that the resonant contributions to the E_1^+ and S_1^+ amplitudes are forbidden by the quark model.[41] Although this lends some interest to the tentative interpretation of the observed scalar-transverse interference term, such a violation of the quark model has already been suggested by photoproduction data for the E_1^+ amplitude.[37]

Although the use of the parameter A in the phenomenological analysis may produce less reliable results because of the possibility of large scalar terms, it is interesting to examine the results obtained using A, along with C and F, to solve directly for $|M_1^+|^2$, $\mathrm{Re}(M_1^+)(E_1^+)^*$, and $\mathrm{Re}(M_1^-)(M_1^+)^*$. Neglecting all terms in A except those involving at least the first power of M_1^+, the results shown in Table VI are obtained. The errors shown are purely statistical and do not include the additional normalization error of approximately 10%.

The results for $\mathrm{Re}(M_1^+)(E_1^+)^*$ and $|M_1^+|^2$ are essentially the same as those obtained from C and F. This fact lends some credibility to the results presented for $\mathrm{Re}(M_1^+)(M_1^-)^*$, but these may be unreliable because

[40] L. D. Roper, R. M. Wright, and B. T. Feld, Phys. Rev. 138, B190 (1965).

[41] C. Becchi and G. Morpurgo, Phys. Letters 17, 352 (1965).

TABLE VI. Multipole amplitudes in the reaction $e^-+p \to e^-+p+\pi_0$. $|M_1^+|^2$, $\mathrm{Re}(E_1^+)(M_1^+)^*$, and $\mathrm{Re}(M_1^-)(M_1^+)^*$ derived from the phenomenological parameters A, C, and F.

q^2 (GeV/c)^2	W (GeV)	$(\bar{\pi}W/MK)\,\lvert M1^+\rvert^2$ (μb/sr)	$\mathrm{Re}(E_1^+)(M_1^+)^*/\lvert M_1^+\rvert^2$	$\mathrm{Re}(M_1^+)(M_1^-)^*/\lvert M_1^+\rvert^2$
0.0463	1.223	17.7 ±0.7	−0.090±0.024	−0.02±0.03
0.0475	1.197	11.7 ±0.6	−0.097±0.037	−0.02±0.05
0.127	1.270	10.5 ±0.3	+0.01 ±0.04	+0.08±0.05
0.130	1.226	12.7 ±0.3	+0.05 ±0.03	+0.02±0.04
0.132	1.183	4.73±0.14	+0.12 ±0.03	−0.12±0.03
0.240	1.321	4.75±0.15	−0.03 ±0.03	−0.07±0.04
0.243	1.284	6.84±0.16	−0.08 ±0.02	−0.06±0.03
0.245	1.259	9.9 ±0.2	−0.06 ±0.02	−0.08±0.02
0.247	1.228	11.3 ±0.2	−0.04 ±0.02	−0.05±0.03
0.250	1.200	10.2 ±0.2	−0.05 ±0.02	−0.15±0.02
0.252	1.166	6.02±0.35	−0.03 ±0.05	−0.18±0.05
0.398	1.278	9.17±0.33	−0.06 ±0.03	−0.03±0.04
0.404	1.232	13.5 ±1.0	−0.10 ±0.04	−0.13±0.04

of the large number of multipoles neglected in A. However, there are certainly no positive indications of large scalar terms in A.

B. $\gamma N\Delta$ Transition Form Factor

If the $\Delta(1236)$ is viewed as a real particle produced via a magnetic dipole transition, the four-momentum transfer dependence of the M_1^+ amplitude can be related to a phenomenological form factor $G_M^*(q^2)$. Several definitions of $G_M^*(q^2)$ appear in the literature. In the notation of Ash *et al.*,[38] the form factor contains the complete four-momentum transfer dependence of the amplitude, with the exception of a factor of $\bar{q}^*$, the photon c.m. momentum which expresses the threshold behavior of the amplitude. From Eqs. (16) and (17) the magnetic dipole contribution to the cross section is

$$d\sigma/d\Omega_\pi = (|\bar{\pi}^*|W/MK)\,|M_1^+|^2 \times(\tfrac{5}{2}-\tfrac{3}{2}\cos^2\theta_\pi^*-\tfrac{3}{2}\epsilon\sin^2\theta_\pi^*\cos 2\phi_\pi). \quad (21)$$

With the present definition of Γ_T, Eq. (4) of Ash *et al.* becomes

$$\frac{d\sigma}{d\Omega_\pi}=\frac{|\bar{q}^*|W}{MK}\left[\tfrac{2}{3}\alpha\left(\frac{G_M^*}{2M}\right)^2|\bar{q}^*|\frac{\sin^2\delta}{\Gamma}\right] \times(\tfrac{5}{2}-\tfrac{3}{2}\cos^2\theta_\pi^*-\tfrac{3}{2}\epsilon\sin^2\theta_\pi^*\cos 2\phi_\pi), \quad (22)$$

so that

$$G_M^*(q^2)=2M\left(\frac{3}{2\alpha}\frac{|\bar{\pi}^*|\Gamma}{\sin^2\delta}\frac{|M_1^+|^2}{|\bar{q}^*|^2}\right)^{1/2}. \quad (23)$$

The present measurement of $G_M^*(q^2)$ is based upon the reaction $(e^-+p)\to(e^-+\Delta)\to(e^-+p+\pi^0)$ and the factor of $\frac{2}{3}$ in Eq. (22) accounts for the assumed branching ratio of the Δ to the π^0+p final state. Γ is the width of the resonance (120 MeV) and δ is the $(\frac{3}{2},\frac{3}{2})$ phase shift.[40] $G_M^*(0)$ is related to the photoproduction matrix element μ^*, calculated by Dalitz and Sutherland[42] by the equation

$$G_M^*(0)=(M/W)^{1/2}\mu^*. \quad (24)$$

From an analysis of photoproduction data, Dalitz and Sutherland obtained $\mu^*=(1.28\pm0.02)\times(2\sqrt{\frac{2}{3}})\mu_p$, where $\mu_p=2.79$. Using Eq. (4), $G_M^*(0)=2.93\pm0.05$. Ash *et al.* obtained $G_M^*(0)=3.00\pm0.01$ by fitting the photoproduction data of Fischer *et al.*[43] These results are to be compared with the prediction of current algebra and $SU(6)$ symmetry, $G_M^*(0)=2.3$,[44] and the result of a recent current-algebra calculation by Barnes and Williams,[45] $G_M^*(0)=3.5$. Barnes and Williams state that the latter value is expected to be an overestimate of $G_M^*(0)$.

The form factor C_3 defined by Dufner and Tsai is related to G_M^* by

$$G_M^*(q^2)=(\sqrt{\tfrac{2}{3}})M\left(\frac{M+W}{W}\right)\times\left[1+\frac{q^2}{(M+W)^2}\right]^{1/2}C_3(q^2). \quad (25)$$

Their form factor $C_3(q^2)$ appears as the coupling constant for one of the three invariant forms of the interaction used in the isobar model. For the purposes of this discussion, C_3 and G_M^* differ primarily in normalization since the additional four-momentum transfer dependence implied by the square-root factor in Eq. (25) differs from unity by less than 4% at four-momentum transfers below 0.4 (GeV/c)^2.

The values for $G_M^*(q^2)$ have been determined by averaging over the resonance. Since the M_1^-, M_1^+ interference term changes sign at resonance, its effect on G_M^* was negligible at $q^2=0.13$ and 0.25 (GeV/c)^2. The correction caused by this term raised the value of G_M^* by 4% at $q^2=0.05$ (GeV/c)^2 and lowered it by 3% at 0.4 (GeV/c)^2. The present values of $G_M^*(q^2)$ are compared with the measurements of Ash *et al.* in Fig. 12.

[42] R. H. Dalitz and D. G. Sutherland, Phys. Rev. **146**, 1180 (1966).

[43] G. Fischer, H. Fischer, H. J. Kampgen, G. Khop, P. Schultz, and H. Wessels, in *Proceedings of the Thirteenth Annual International Conference on High-Energy Physics, Berkeley, 1966* (University of California Press, Berkeley, 1967).

[44] Quoted by K. J. Barnes and R. M. Williams (Ref. 45).

[45] K. J. Barnes and R. M. Williams, Nucl. Phys. **B3**, 424 (1967).

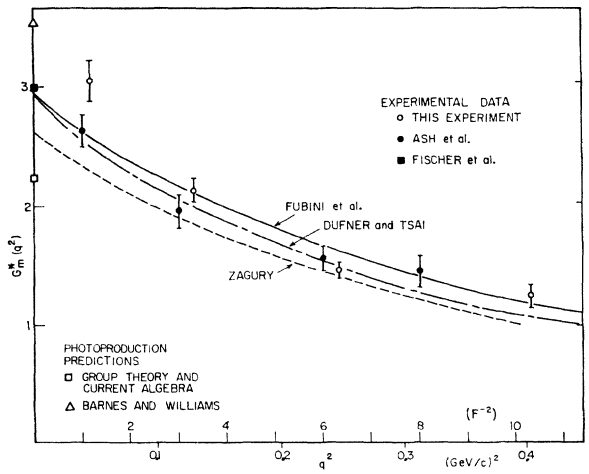

FIG. 12. The $\gamma N\Delta$ form factor.

The agreement is generally good except for our lowest four-momentum transfer point, which appears high when compared with the more precise photoproduction data. Also shown in the figure are the form-factor dependence obtained by Dufner and Tsai,[39] the prediction of the static theory of Fubini *et al.*[22] and the phenomenological form factor implied by the fully relativistic dispersion theory of Zagury.[12] The latter curve is taken from Fig. 2 of Ash *et al.* Clearly, the static-theory prediction of a form factor proportional to the nucleon magnetic isovector form factor is approximately correct in this region of four-momentum transfer, as concluded by Ash *et al.* The data are also consistent with the exponential form-factor dependence suggested by Dufner and Tsai and Bartel *et al.*[7] on the basis of their analysis of inelastic electron-proton scattering experiments in which only the scattered electron was detected.

VIII. PION FORM FACTOR

The π^+ data were fitted with the dispersion theories of Adler[24] and of Zagury[12] using the pion form factor as a free parameter. Although the two theories are almost idential in the photoproduction limit, significant numerical differences exist at four-momentum transfers below 0.6 $(GeV/c)^2$. For this reason, the analysis has been carried out for both theories. The results are presented separately and should serve as a qualitative estimate of additional model-dependent theoretical uncertainties not considered in Ref. 11.

The cross section for single-pion electroproduction is given by Eq. (5). The scalar cross section $d\sigma_0/d\Omega_\pi$ is dominated by a term proportional to the square of the pion form factor and is estimated to contribute between 37 and 68% of the observed cross section, depending on the c.m. energy and four-momentum transfer. Akerlof *et al.*[11] assumed a 5% theoretical uncertainty in this term to allow for effects such as the modification of the OPE amplitude due to final-state interactions. We view this as reasonable and have also assumed a 5% error in $d\sigma_0/d\Omega_\pi$.

In Sec. VII the presence of a scalar-transverse interference term in the π^0 cross section, which is expected to be insensitive to the pion form factor, was discussed. This is interpreted at present as being caused by the interference of the M_1^+ amplitude with the scalar quadrupole S_1^+ amplitude. If the latter were as large in the π^+ cross section, its contribution to $d\sigma_0/d\Omega_\pi$ would be approximately 5%.

For π^+ production, the scalar-transverse term $S(\theta_\pi^*)$ is very sensitive to F_π, but is highly model-dependent, because the interference between the real pion-pole term and the resonant (imaginary) magnetic dipole amplitude is small. The size of the $\cos\phi_\pi$ term is therefore dependent on which of the smaller, predominantly real, transverse multipole amplitudes are included in the theory. However, since the data span a wide range of ϕ_π, the effects of this term tend to integrate out and the pion form-factor analysis is almost entirely dependent on the more reliably calculable $d\sigma_0/d\Omega_\pi$. However, the observation of the $\cos\phi_\pi$ dependence of the cross section serves as a qualitative test of the theories.

No additional theoretical error was assigned to the $\cos\phi_\pi$ term, or to the $\cos 2\phi_\pi$ term, which was small in the angular region covered by the measurements.

The error in the transverse cross section was estimated from the discrepancies between the theoretical predictions and the photoproduction data tabulated by Beale *et al.*[46] On the basis of this comparison, an error of between 4 and 30% was assigned to $d\sigma_T/d\Omega_\pi$ depending on the pion-nucleon c.m. energy and the pion c.m. polar angle. In the photoproduction limit both Adler and Zagury tend to overestimate $d\sigma_T/d\Omega_\pi$ in the extreme forward direction at energies above the resonance. This overestimate becomes worse with increasing W. The agreement between theory and experiment improves as θ_π^* increases. For this reason data forward of 10° c.m. have been excluded from the fits at all energies above 1225 MeV. These data usually had rather large errors, so that this procedure had little effect on the fits.

Since the ratio $R_{S-T} \equiv (d\sigma_0/d\Omega_\pi)/(d\sigma_T/d\Omega_\pi)$ decreases with θ_π^*, most data sets were divided into two subsets, one at small angles and one at large angles. The two determinations of F_π obtained from each set were weighted and averaged. However, they provided an intermediate check on the consistency of the predicted distribution in polar angle. One outstanding inconsistency was found at $q^2=0.13$ $(GeV/c)^2$, $W=1185$ MeV. For this data set the pion form-factor value extracted from the forward-angle data at 12° c.m. was considerably higher than that implied by the large-angle data. The $q^2=0.12$ $(GeV/c)^2$ form factor value

[46] J. T. Beale, S. D. Eklund, and R. L. Walker, Caltech Synchrotron Lab Report No. CTSL-42, 1966 (unpublished).

TABLE VII. Best-fit values for the pion form factor. Separation into pion polar angle bins.

q^2 (GeV/c)^2	W (GeV)	No. of points	A	χ^2 Z	F_π Adler, expt	F_π Zagury, expt	$\Delta\left(\frac{d\sigma}{d\Omega_\pi}\right)_{\text{theor}}$	θ_π*
0.048	1170	21	28	30	0.96±0.07	0.83±0.07	7.4%	6°–33°
0.047	1197	19	19	18	1.03±0.12	0.94±0.09	7.2%	6°–33°
0.046	1223	17	22	20	0.93±0.05	0.96±0.15	3.3%	6°–41°
0.132	1183	5	1.0	1.5	0.7 ±0.11	0.54±0.1	7.3%	12°
0.132		13	7.7	6.8	$0.3_{-0.16}^{+0.15}$	0.26±0.12	6.4%	20°–40°
0.130	1226	6	1.7	2.3	$0.49_{-0.19}^{+0.16}$	$0.57_{-0.16}^{+0.15}$	5.5%	12°
0.130		13	18	16	$0.47_{-0.47}^{+0.14}$	$0.63_{-0.16}^{+0.12}$	5.7%	20°–35°
0.127	1270	7	5.5	5.2	$0.67_{-0.18}^{+0.14}$	$0.79_{-0.21}^{+0.14}$	15.0%	12°
0.127		14	25	26	$0.71_{-0.17}^{+0.12}$	$0.80_{-0.15}^{+0.13}$	13.0%	20°–40°
0.250	1200	14	12.5	11.5	0.64±0.1	0.54±0.08	5.8%	9°–25°
0.250		11	19	21	0.3 ±0.4	0.50±0.11	5.6%	35°–44°
0.245	1259	14	19	18	$0.38_{-0.24}^{+0.16}$	$0.59_{-0.18}^{+0.12}$	13.0%	15°–25°
0.245		12	19	20	$0.52_{-0.22}^{+0.19}$	0.70±0.16	14.2%	35°–44°
0.404	1238	14	12	11	0.0 ±0.4	$0.45_{-0.22}^{+0.10}$	9.4%	15°–24°
0.404		7	5.5	3	$0.3_{-0.3}^{+0.2}$	$0.66_{-0.18}^{+0.11}$	6.0%	34°–43°
0.398	1278	7	5.5	4.5	0.5 ±0.13	$0.67_{-0.14}^{+0.13}$	19.1%	15°–25°
0.398		7	2.8	3.0	0.6 ±0.12	$0.75_{-0.14}^{+0.1}$	17.5%	35°–42°

TABLE VIII. Averaged values of the pion form factor at each pion-nucleon c.m. energy and four-momentum transfer.

q^2 (GeV/c)^2	W (GeV)	Adler theory F_π (expt)	Adler theory ΔF_π (tot)	Zagury theory F_π (expt)	Zagury theory ΔF_π (tot)
0.048	1170	0.96±0.07	±0.09	0.83±0.07	±0.09
0.047	1197	1.03±0.12	±0.15	0.94±0.09	±0.11
0.046	1223	0.93±0.05	±0.05	0.96±0.15	±0.16
0.132	1183	0.57±0.09	±0.13	0.43±0.08	±0.11
0.130	1226	$0.48_{-0.18}^{+0.11}$	$_{-0.23}^{+0.14}$	$0.61_{-0.11}^{+0.09}$	$_{-0.14}^{+0.12}$
0.127	1270	$0.69_{-0.12}^{+0.09}$	$_{-0.27}^{+0.20}$	$0.80_{-0.12}^{+0.10}$	$_{-0.24}^{+0.23}$
0.250	1200	0.62±0.09	±0.10	0.53±0.06	±0.08
0.245	1259	$0.45_{-0.16}^{+0.12}$	$_{-0.35}^{+0.26}$	$0.64_{-0.12}^{+0.10}$	$_{-0.26}^{+0.21}$
0.404	1232	$0.22_{-0.19}^{+0.18}$	$_{-0.32}^{+0.26}$	$0.56_{-0.14}^{+0.08}$	$_{-0.20}^{+0.11}$
0.398	1278	0.55±0.09	±0.24	$0.72_{-0.10}^{+0.08}$	$_{-0.28}^{+0.23}$

obtained by Akerlof *et al.* was dominated by measurements in this energy region at $\theta_\pi^*=0°$. Their value is even higher than the value obtained from the present data at 12° c.m. If this trend is due to an incorrect prediction of the angular distribution in θ_π^*, the discrepancy between the present value of F_π at $q^2=0.13$ (GeV/c)^2 and that obtained by Akerlof *et al.* could be theoretical rather than experimental in origin.

Table VII shows the best fit values for F_π in each region of pion polar angle for both theories. Also shown are the experimental errors, the minimum values of χ^2 for each data set, and the estimated error in the theoretical cross section.

Difficulties associated with the pion-proton separation limited the measurements at $q^2=0.6$ (GeV/c)^2 to c.m. energies near 1290 MeV. In this region, the uncertainty in the calculated value of $d\sigma_T/d\Omega_\pi$ was estimated to be of the same order as $d\sigma_0/d\Omega_\pi$ so that a meaningful determination of F_π was not possible.

Table VIII shows the averaged values for F_π at each c.m. energy, and the experimental and total errors. In the averaging, theoretical errors associated with the large- and small-angle data were assumed to be completely correlated.

For each region of four-momentum transfer the values for F_π associated with different values of W were averaged. Once again the theoretical errors were assumed to be completely correlated. The results are listed in Table IX and shown in Fig. 13.

Also shown in Fig. 13 are the results of Akerlof *et al.*,[11] the prediction of the ρ-dominance model, and the q^2 dependence of the nucleon form factors, normalized to unity at $q^2=0$. The errors on the present results are, in most cases, dominated by the theoretical error. Since the theory is constantly being refined, this situation should be temporary, and a more reliable estimate of

TABLE IX. Electroproduction estimates of the pion form factor.

q^2 (GeV/c)	Adler theory	Zagury theory
0.05	0.95±0.05	0.89±0.08
0.13	$0.56_{-0.10}^{+0.09}$	0.54±0.08
0.25	$0.61_{-0.10}^{+0.09}$	0.54±0.08
0.40	$0.41_{-0.19}^{+0.18}$	$0.60_{-0.16}^{+0.10}$
	Akerlof *et. al.*	
0.04	$0.79_{-0.18}^{+0.16}$	
0.12	0.82±0.06	
0.23	$0.57_{-0.09}^{+0.08}$	

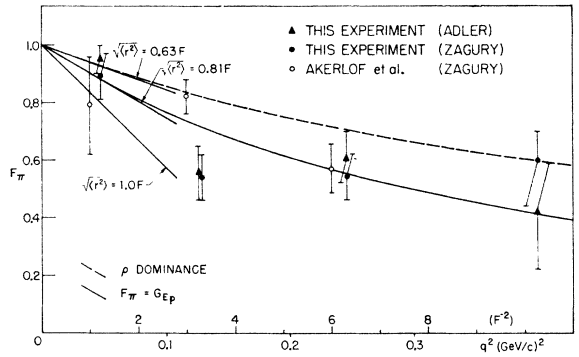

FIG. 13. The pion form factor.

the pion form factor from the present data may well be obtainable in the future. The results suggest that the pion form factor is similar to that of the proton, but are too imprecise to exclude ρ-dominance behavior.

However, if it can be assumed that the form-factor dependence is smooth at small four-momentum transfers, then it is apparent that the value of the rms pion charge radius, given by $\langle r^2\rangle^{1/2}=[(-6dF_\pi/dq^2)_{q^2=0}]^{1/2}$, lies between the limits of 0.63 and 1.0 F indicated in Fig. 13. A fit to the seven form factor values analyzed using Zagury's theory (four from the present work and three from Akerlof *et al.*) yields a charge radius of $\langle r^2\rangle^{1/2}=0.86\pm0.09$ F if the fitting function is assumed to be $F_\pi=1/(1+q^2/m^2)$ as suggested by ρ dominance. This fit had a χ^2 of 9 for six degrees of freedom. The corresponding mass was $M=560\pm60$ MeV.

Similar fits using the present form-factor values give $\langle r^2\rangle^{1/2}=0.84\pm0.10$ F, $M=577\pm70$ MeV using the four form-factor values obtained with Adler's theory, and $\langle r^2\rangle^{1/2}=0.95\pm0.11$ F, $M=507\pm60$ MeV using the form-factor values obtained with Zagury's theory. If the differences in the values of $\langle r^2\rangle^{1/2}$ and M are taken as an indication of the additional model-dependent errors and are added in quadrature with the previously quoted errors, the final values obtained for the rms radius and vector meson mass, from the seven Zagury values, are

$$\langle r_\pi^2\rangle^{1/2}=0.86\pm0.14\text{ F},\quad M=560\pm80\text{ MeV}.$$

Fits using a protonlike form factor $F_\pi=1(1+q^2/A)^2$ yielded a charge radius similar to the above.

Previous measurements of the pion charge radius have given $\langle r_\pi^2\rangle^{1/2}=2.96\pm0.43$ F [47] and $\langle r_\pi^2\rangle^{1/2}<0.9$ F [48] from $\pi^\pm-\alpha$ scattering, and $\langle r_\pi^2\rangle^{1/2}<3$ F [49,50] from π-e scattering. Therefore, until accurate π-e scattering experiments can be performed at the Serpukov or N.A.L. accelerators, electroproduction appears to provide the most reliable experimental estimate of this quantity.

IX. SUGGESTIONS FOR FUTURE EXPERIMENTS

The present experiment employed a large-solid-angle coincidence array, without momentum analysis of the detected particle, because much of the apparatus was already available. Nevertheless, the large solid angle was a definite advantage in what was intended to be a general survey of single-pion electroproduction in the vicinity of the $\Delta(1236)$ resonance at low four-momentum transfers.

However, approximate calculations indicate that a coincident-particle spectrometer with a solid angle of 20 msr and a momentum acceptance $\Delta p/p$ of 20%, would have a background counting rate of approximately 3% of that in the present coincidence array. The use of a time–to–pulse-height unit to measure the time interval between the arrival of the electron and the coincident particle would also permit a reduction in the random-coincidence rate. Employed together, these techniques should allow at least a sixfold increase in the rate of data accumulation. The use of a suitable coincidence particle spectrometer should also enable the measurements to be extended to higher four-momentum transfers and to forward pion angles in the reaction $e^-+p\rightarrow e^-+p+\pi^0$.

The precision with which the dispersion theories predict the π^0 electroproduction angular distribution at resonance, and the π^+ photoproduction angular distribution for $30°<\theta_\pi^*<60°$, suggest that more accurate measurements of F_π, at four-momentum transfers less than 0.3 $(\text{GeV}/c)^2$, might be obtained by performing precise cross-section measurements in favorable kinematic regions. The requirements for an accurate estimate of F_π are, first, that $\epsilon(d\sigma_0/d\Omega_\pi)/(d\sigma_T/d\Omega_\pi)$ should be large, and, secondly, that the theoretical estimates of $d\sigma_T/d\Omega_\pi$ should be reliable. The first criterion implies $\epsilon\simeq1$, $W<1240$ MeV, and $\theta_\pi^*<40°$. However, the existing electroproduction theories[12,24] predict a large forward peak in the reaction $\gamma+p\rightarrow\pi^++n$, which is not observed in practice. The agreement is better for c.m. energies below the resonance, but is typically 20% at $\theta_\pi^*=0$. A more recent photoproduction analysis obtains very impressive agreement with the forward π^+ angular distribution at c.m. energies up to 1300 MeV, but has not yet been extended to electroproduction. Until this is done, a more favorable angular region for determining the pion form factor would appear to be $30°<\theta_\pi^*<45°$, where $d\sigma_0/d\Omega\simeq d\sigma_T/d\Omega$, provided $W<1240$ MeV, and the theoretical estimates of the transverse cross section are in good agreement with experiment. Unfortunately, even in this region the predicted values[12,13] of the transverse cross section diverge rapidly as a function of four-momentum transfer, a 10% difference at $q^2=0$ becoming $\simeq30\%$ at $q^2=0.4$ $(\text{GeV}/c)^2$.

[47] K. M. Crowe, A. Fainberg, J. Miller, and A. S. L. Parsons, Phys. Rev. **180**, 1349 (1969).
[48] M. M. Block, I. Kenyon, J. Kern, D. Koetke, P. Malhotra, R. Walker, and H. Winzeler, Phys. Rev. **169**, 1074 (1968).
[49] J. Allan, G. Ekspong, P. Sallstrom, and K. Fischer, Nuovo Cimento **32**, 1144 (1964).
[50] D. Cassel, M. Barton, R. Crittenden, V. Fitch, and L. Leipuner (unpublished).

Therefore, until the theories are improved significantly more accurate estimates of F_π cannot be expected from this technique.

A more ambitious experimental program, which is less model-dependent, is to attempt to isolate the longitudinal part of the cross section by measuring the angular distribution as a function of ϵ. However, precise large-angle coincidence measurements are extremely difficult at the present time.

Both the approaches outlined above need to assume the dominance of the longitudinal part of the cross section by the OPE term in order to determine F_π, a disadvantage which is not present in Frazer's suggestion[10] of an extrapolation to the pion pole. This procedure still appears to be impractical for c.m. energies near the $\Delta(1236)$ resonance since the pole moves rapidly away from the physical region as the four-momentum transfer is increased. At the resonance peak, for example, the pole is at $\cos\theta_\pi^*=1.15$ in photoproduction and at $\cos\theta_\pi^*=1.6$ for $q^2=0.6$ $(\mathrm{GeV}/c)^2$. The procedure is complicated by the fact that the extrapolation function is not linear in $\cos\theta_\pi^*$.[51] However, recent π^+ photoproduction angular distributions for E_γ between 5 and 16 GeV [52] show a distinct, narrow peak in the forward direction, which may be associated with the pion-pole contribution. Since, at fixed q^2, the pole moves toward the physical region as W is increased, an extrapolation at high pion-nucleon c.m. energies should be considered.

Goryachkin and Semikos[53] have suggested determining the pion form factor from a measurement of π^+ electroproduction with a polarized proton target. Such experiments have recently become feasible through the development of polarized target materials[54] more resistant to radiation damage than the conventional lanthanum magnesium nitrate. The asymmetry in the triply differential cross section with the target polarization parallel and antiparallel to the electron scattering plane can be written

$$\frac{(d\sigma/d\Omega)_\uparrow-(d\sigma/d\Omega)_\downarrow}{(d\sigma/d\Omega)_\uparrow+(d\sigma/d\Omega)_\downarrow}=P\frac{(d\sigma/d\Omega)_p}{(d\sigma/d\Omega)_\pi},$$

where $d\sigma/d\Omega_p$ can be written as the imaginary part of a sum of a product of multipole amplitudes, $(d\sigma/d\Omega)_\pi$ is the unpolarized cross section, and P is the polarization of the target.

The critical point of this suggestion is that $d\sigma/d\Omega_p$ is expected to be dominated by interferences between the real Born terms involving the pion form factor and the large, predominantly imaginary M_1^+ amplitude. If a 10% calculation of $d\sigma/d\Omega_p$ proves to be possible and the target polarization can be determined to the same precision, this method should permit measurements of F_π with useful accuracy.

ACKNOWLEDGMENTS

It is a pleasure to acknowledge the assistance provided by the staffs of the Harvard University Cyclotron Laboratory and the Cambridge Electron Accelerator during the preparation and execution of this experiment. G. Thomson, L. Beardsley, and P. Julien helped with the construction of several items of apparatus and during the data taking. J. Alberi and A. Litke wrote indispensible data-analysis programs for the PDP-1 computer. H. Jones aided our understanding of many theoretical questions during the early stages of the experiment. N. Dombey provided invaluable advice on theoretical topics during data analysis. We are grateful to S. Adler and N. Zagury for informative discussions and for copies of computer programs for calculating their dispersion-theory predictions. K. Berkelman made several useful suggestions; we appreciate his stimulating interest throughout the experiment.

[51] J. G. Taylor, M. J. Moravcsik, and J. L. Uretsky, Phys. Rev. **113**, 689 (1959).

[52] B. Richter, in *Proceedings of the 1967 International Symposium on Electron and Photon Interactions at High Energies* (Stanford Linear Accelerator Center, Stanford, Calif., 1967), p. 309. Int. Union Pure and Applied Phys. Report No. CONF.-670923 (unpublished).

[53] V. G. Goryachkin and V. B. Semikos, Joint Institute for Nuclear Research (Dubna) Report No. P2-3774, 1968 (unpublished).

[54] R. J. Wagner and R. P. Haddock, Phys. Rev. Letters **16**, 1116 (1966). M. Borghini, S. Mango, O. Rurolfsson, and J. Vermeuler, in Proceedings of the International Conference on Polarized Targets and Ion Sources, Saclay, 1966 (unpublished); J. R. Chen, R. V. Pound, J. Sanderson, and C. Zajde, Rev. Sci. Instr. (to be published).

Errata

Nature of $SU(3)\times SU(3)$ Symmetry Breaking – Results from a Systematic Test of the Soft-Meson Theorems, Frank von Hippel and Jae Kwan Kim [Phys. Rev. D 1, 151 (1970)].

Eq. (1.3): The right-hand side should have its sign reversed.

Eq. (3.7): The term on the right-hand side proportional to $\mathfrak{M}_\alpha - \mathfrak{M}_\beta$ should have its sign reversed.

Eqs. (4.4) and (4.6): A dot indicating a time derivative is missing over the $A^0_\alpha(0)$ on the left-hand side.

Eq. (4.17): This equation should read

$$\dot{A}^0_\alpha \to +[\sqrt{\tfrac{2}{3}} + cd_{8\alpha\alpha}]v_\alpha, \quad \alpha \neq 8 .$$

Eq. (A11): The right-hand side should be multiplied by 3.

Table I: The experimental πN scattering lengths were quoted in pion Compton wavelengths rather than fermis. They should therefore be multiplied by ≈ 1.4.

Table II: In the column under "Experimental values" the πN entries become

$$(\pi N)_{1/2}: 0.06 \pm 0.01, \quad (\pi N)_{3/2}: -0.01 \pm 0.01 ,$$

because of the error in Table I.

Table III: In the column under $\Delta \mathrm{Re}T$, the πN entries become

$$(\pi N)_{1/2}: 0.02 \pm 0.03, \quad (\pi N)_{3/2}: -0.05 \pm 0.03 ,$$

also because of the error in Table I. The values in the column under T_A should be multiplied by a factor of 3 because of the error in Eq. (A.11).

Most of the sign errors occurred in the change of sign convention for $\mathfrak{M}$ from our earlier Letter[1] to the article. They, therefore, do not affect our numbers. The numerical errors are minor and do not affect our conclusions. We are indebted to Robert Cahn for bringing most of these errors to our attention.

[1] F. von Hippel and J. K. Kim, Phys. Rev. Letters 22, 740 (1969).

General Local Interactions and Tests of $V-A$ Theory in Neutrino Scattering Processes, T. P. Cheng and Wu-Ki Tung [Phys. Rev. D 3, 733 (1971)]. Factors of $\frac{1}{2}$ should be omitted in the expression for I_8 and I_9 in Eq. (38). In Eq. (49), J's should be replaced by V's in expressions for a_2 and a_3. In Eq. (A1), a term $T_{(m)\sigma'\sigma}$ should be inserted after the factor $\sqrt{2}\, m_l(1+m_l^2/q^2)^{1/2}$. In the last paragraph of Appendix C, the correct equation should read $3a_1 = b_1$.

Possible Test of the $\Delta S = \Delta Q$ Rule in $K^0_{\mu 3}$ Decay in a Regeneration Experiment, Abdul Ebrahim [Phys. Rev. D 3, 109 (1971)]. The last expression following Eq. (4) should read

$$G_2 = (m/2M)[(f_+ - f_-) - r(g_+ - g_-)].$$

Coincidence Measurements of Single-Pion Electroproduction near the $\Delta(1236)$ Resonance, C. Mistretta, J. A. Appel, R. J. Budnitz, L. Carroll, J. Chen, J. R. Dunning, Jr., M. Goitein, K. Hanson, D. C. Imrie, and Richard Wilson, [Phys. Rev. 184, 1487 (1969)]. The overall sign of the $(M_1^-)(M_1^+)^*$ interference term in the A coefficient on page 1500 should be positive instead of negative. The numbers presented in Table VI are slightly altered and can be recalculated using Table IV and Eqs. (17). We wish to thank J. Gayler for bringing this to our attention.